Biomass-burning derived particles from a wide variety of fuels: Part 1: Properties of primary particles

Crystal D. McClure[1], Christopher Y. Lim[2,%], David H. Hagan[2], Jesse H. Kroll[2], Christopher D. Cappa[1,3,*]

[1] Department of Civil and Environmental Engineering, University of California, Davis, CA 95616
[2] Department of Civil and Environmental Engineering, Massachusetts Institute of Technology, Cambridge, MA, USA
[3] Atmospheric Sciences Graduate Group, University of California, Davis, CA, USA 95616
[%] Now at Department of Chemistry, University of Toronto, Ontario, Canada

[*] To whom correspondence should be addressed: cdcappa@ucdavis.edu

ABSTRACT

Relationships between various optical, physical, and chemical properties of biomass combustion derived particles are characterized for particles produced in the laboratory from a wide range of fuels and burn conditions. The modified combustion efficiency (MCE), commonly used to parameterize biomass particle emissions and properties, is shown to generally have weak predictive capabilities, especially for more efficient combustion conditions. There is, however, a strong relationship between many intensive optical properties (e.g. single scatter albedo, Ångstrom absorption exponent, mass absorption efficiency) and the organic aerosol-to-black carbon ([OA]/[BC]) mass ratio over a wider range than previously considered (0.3 to 10^5). The properties of brown carbon (BrC, i.e. light absorbing organic carbon) also vary with [OA]/[BC]. Coating-induced enhancements (i.e., "lensing" effects) contribute only a minor amount to BC absorption for all of the burns despite some burns producing particles having large ensemble-average coating-to-core mass ratios. The BC-OA mixing state varies strongly with [OA]/[BC]; the fraction of OA that is internally mixed with BC decreases with [OA]/[BC] while the relative amount of OA coated on BC increases. In contrast, there is little relationship between many OA bulk chemical properties and [OA]/[BC], with the O:C and H:C atomic ratios and the relative abundance of a key marker ion (m/z = 60, linked to levoglucosan) all showing no dependence on [OA]/[BC]. In contrast, both the organic nitrate fraction of OA and the OA volatility do depend on the [OA]/[BC]. Neither the total particle or BC-specific size distributions exhibit any clear dependence on the burn conditions or [OA]/[BC], although there is perhaps a dependence on fuel type. Overall, our results expand on

existing knowledge to contribute new understanding of the properties of particles emitted from biomass combustion.

1 Introduction

While it is understood that both open and controlled biomass combustion are major sources of particles to the atmosphere (Andreae and Merlet, 2001), questions remain regarding the properties of the emitted particles, their relationship with combustion conditions and fuel type, and their atmospheric evolution. Particles emitted from biomass combustion impact the global radiation budget and contribute to poor air quality in impacted regions. The emitted primary particles are primarily composed of organic aerosol (OA) and black carbon (BC), in varying amounts, with trace inorganic species (Reid et al., 2005;McMeeking et al., 2009;Levin et al., 2010). Particle intensive properties are often compared against the modified combustion efficiency (MCE ~ $\Delta[CO_2]/(\Delta[CO]+\Delta[CO_2])$), which provides a measure of the combustion efficiency of a burn. For example, various particle properties show some relationship with MCE, but often these relationships are weak, especially for more efficient combustion (higher MCE, corresponding typically to flaming conditions) (McMeeking et al., 2009;Liu et al., 2013;McMeeking et al., 2014). Understanding the diversity in the chemical, physical, and optical properties of the emitted particles is important for establishing the fire- or region-specific emissions and subsequent impacts.

The emitted OA from biomass combustion is somewhat light absorbing (Kirchstetter et al., 2004). Absorbing OA is commonly referred to as brown carbon (BrC), with properties that appear to depend on the fuel and combustion conditions (Saleh et al., 2014;Laskin et al., 2018), which affect particle organic composition (Jen et al., 2019). However, the properties of primary BrC absorption and, especially, understanding of the relationships between BrC absorption and other particle properties and burn conditions is only beginning to be unraveled. Additionally, it is established from theory and laboratory experiments that non-absorbing coatings on black carbon and other strongly absorbing particles can enhance the absorption (commonly referred to as the "lensing" effect but more accurately termed here the coating-induced enhancement) (Fuller et al., 1999;Bond et al., 2006;Lack et al., 2009;Shiraiwa et al., 2010;Cappa et al., 2012). Yet, the extent to which coating-induced enhancements impact absorption by ambient particles or for mixed-

component particles from complex sources, such as biomass burning, remains contentious (Cappa et al., 2012;Healy et al., 2015;Liu et al., 2015;Peng et al., 2016;Liu et al., 2017).

Here, we expand on current understanding of the relationships between various primary particle properties and burn conditions by analyzing measurements of primary biomass burning particles produced from combustion of a variety of fuel types, many of particular relevance to the western U.S.. We demonstrate that various optical properties exhibit a strong relationship with the [OA]/[BC] mass ratio, much stronger than their relationship with the MCE. We use the measurements to quantify the individual contributions of BC, BrC and from internal mixing of BC to the observed light absorption, and examine the variability in the properties of BrC specifically. We uniquely characterize the mixing state of BC and OA, and how mixing state vary between individual burns and depend on the mean properties of the emitted particles. We characterize the variability of OA-specific properties, including OA volatility, bulk chemical composition (characterized by the O:C and H:C atomic ratio, and the presence of key marker ions), and, uniquely, the relative abundance of organic nitrate species. We also examine the variability in the emitted particle size distribution, both for the total particles and for the BC particles specifically. Some of our analysis serves to support and extend previously determined relationships by considering a wider range of conditions, while other aspects are unique to this study. These observations provide a foundation for understanding and interpretation of experiments on the influence of photochemical aging on biomass particle properties, discussed in a related paper (Lim et al., 2019).

2 Methods

All experiments were conducted during the Fire Influence on Regional to Global Environments Experiment (FIREX) lab study, which took place at the Missoula Fire Sciences Lab in Missoula, MT, USA during November, 2016. Numerous types of biomass were combusted in a large chamber (12 x 12 x 19 m) and the smoke sampled to provide information on the physical, chemical, and optical properties of the resulting smoke (i.e., particulate and gas emissions). The general fuels types combusted included (exclusively or in combination): duff, dung, excelsior, straw, litter, untreated lumber, rotten debris, woody debris, shrub, herbaceous, and canopy biomass. A complete list of fuels and types is provided in **Table S1**, with further details available on the U.S. National Oceanic and Atmospheric Administration (NOAA) data archive

(https://esrl.noaa.gov/csd/projects/firex/). All data used in this publication are also available on the NOAA archive, with the processed data summarized in complementary data repository (Cappa et al., 2019a).

Both "room" and "stack" burns were conducted, although here we include results only from stack burns. During stack burns, the smoke was mixed with background room air and funneled up a large cylindrical stack (2 m dia. x 15 m height) where it was sampled into a high-flow transfer line at ca. 0.27 m^3/s. This flow rate corresponded to sampling approximately 10% of the stack flow. Smoke was transferred to an adjacent room via the high-flow transfer line (residence time ca. 2 s) where it was sub-sampled through a $PM_{2.5}$ cyclone and injected into a 0.25 m^3 Teflon photochemical reaction chamber (the mini chamber). Details on the construction and operation of the mini chamber can be found in (Lim et al., 2019). Here, we focus exclusively on the properties of particles sampled prior to initiation of photochemical oxidation; results of the photochemical oxidation experiments are discussed in a series of papers (Coggon et al., 2019;Lim et al., 2019). In brief, prior to each burn, the chamber was flushed with clean air with a relative humidity (RH) of approximately 40%. To fill the chamber, smoke was sub-sampled from the high-flow inlet and injected across the entire burn (typically lasting for 10-20 minutes) or until the chamber concentration reached a maximum. A suite of instruments sampled from the mini chamber at a flow rate of approximately 6 lpm. This flow rate varied from burn to burn due to the exact suite of instruments sampling. Clean makeup air was being injected simultaneously from a zero air generator to equal the air being sampled out of the chamber. The sampled smoke was diluted by a factor of ca. seven relative to the air in the high-flow inlet. Subsequent dilution after filling was characterized by the decay of acetonitrile (ACN). Properties of the primary particles are averaged over the 5-10 minute period after filling but before the initiation of photochemistry.

Particle-phase instrumentation sampled alternatingly every two minutes through a thermodenuded or ambient sample line. The thermodenuder was operated at 300 ºC with a residence time of approximately 5 s and volatilized semi-volatile components, including those that are internally mixed with BC. The ambient line was lined with a charcoal cloth that removed excess gases (such as VOCs, NO_x, and O_3) that could interfere with particle-phase measurements. Comparison of thermodenuded versus ambient particles allowed for the investigation of coating amount and volatility. The gas-phase composition in the mini chamber was similar to that sampled directly from the fire (Koss et al., 2018;Lim et al., 2019). Particle phase instrumentation included:

a multi-wavelength cavity-ringdown-photoacoustic absorption spectrometer (CRD-PAS) and a photoacoustic absorption spectrometer (PASS-3) for characterization of light absorption and extinction coefficients at 405 nm, 532 nm, and 781 nm; a high resolution aerosol mass spectrometer (HR-ToF-AMS) for characterization of non-refractory submicron particulate matter (NR-PM_1) components (i.e. OA, NO_3, SO_4, NH_4, Cl, K); a soot photometer AMS (SP-AMS) in laser-only mode for characterization of refractory BC and the NR-components that are internally mixed with BC; a single particle soot photometer (SP2) for characterization of refractory BC mass concentrations and size distributions; and a scanning electrical mobility sizer (SEMS) for measurement of particle mobility size distributions. Further details regarding instrument operation and calibration are provided in the Supplemental Material and in Lim et al. (2019).

3 Results and Discussion

3.1 Bulk optical property relationships

Due to the wide variety of biomass fuels and types used during FIREX, there was a substantial diversity in the properties of primary particles produced. Previous studies have shown both the single scatter albedo (SSA) and wavelength-dependence of absorption (the absorption Angstrom exponent, AAE) depend on the modified combustion efficiency (MCE) (Liu et al., 2013;McMeeking et al., 2014;Pokhrel et al., 2017). The MCE is defined here as:

$$\boldsymbol{MCE} = \frac{[\boldsymbol{CO_2}]}{[\boldsymbol{CO_2}]+[\boldsymbol{CO}]} \quad (1)$$

The SSA is defined as:

$$SSA = \frac{b_{ext}-b_{abs}}{b_{ext}} \quad (2)$$

where b_{ext} is the wavelength-specific extinction coefficient and b_{abs} is the wavelength-specific absorption coefficient. The AAE is defined as:

$$AAE = -\log(\frac{b_{abs,\lambda 1}}{b_{abs,\lambda 2}})/\log\left(\frac{\lambda 1}{\lambda 2}\right) \quad (3)$$

where λ_1 and λ_2 indicate two different wavelengths, here 405 nm and 532 nm. The MCE characterizes the overall combustion efficiency, with values closer to unity indicating more

complete combustion. In general, higher MCE correspond to more flaming combustion conditions while smaller MCE correspond to more smoldering conditions. We find a similar relationship between SSA_{405nm}, AAE, and [OA]/[BC] with MCE as previous studies (**Figure 1**) (McMeeking et al., 2009;Liu et al., 2013;McMeeking et al., 2014;Pokhrel et al., 2017). Specifically, the SSA_{405nm} is relatively constant and near unity for MCE < ~0.9, but above this value exhibits a rapid decline, albeit with a substantial amount of scatter (**Figure 1**a). The AAE is also relatively constant when MCE < 0.9, with very large values (AAE ~ 8). There is a rapid, scattered decrease in the AAE as MCE increases further (**Figure 1**b). The relationship between [OA]/[BC] and MCE is similar, with values generally decreasing as MCE increases but a large amount of scatter (**Figure 1**d). There is also a general relationship between the mass absorption coefficient referenced to BC (MAC_{BC}) at 405 nm and the MCE, but with similar scatter as the other properties (**Figure 1**c). The MAC_{BC} is defined as:

$$MAC_{BC} = b_{abs}/[BC] \quad (4)$$

The $MAC_{BC,405nm}$ includes contributions from absorption by BC, BrC, and from coating-induced enhancement of BC absorption. These results, along with the literature, indicate that MCE can provide guidance as to the general magnitude of these particle properties, but that the MCE is ultimately a fairly imprecise metric, especially for the SSA_{405nm}.

However, we find a very strong relationship between the SSA_{405nm} and the total [OA]/[BC] ratio (**Figure 1**e). This is consistent with the findings of Pokhrel et al. (2016), who observed something similar but over a smaller range of [OA]/[BC]. (Similarly strong relationships are observed for SSA values at 532 nm and 781 nm (**Figure S1**), or if the [NR-PM_1]/[BC] are used as OA averages 95% of the total NR-PM_1 mass.) Smaller [OA]/[BC] correspond to smaller SSA_{405nm} values with a sigmoidal relationship observed. (Fit parameters for all fits shown are provided in **Table S1**.) There is similarly a very strong, sigmoidal relationship between the AAE and $MAC_{BC,405nm}$ and [OA]/[BC] (**Figure 1**f,g). The large increase in the $MAC_{BC,405nm}$ indicates that BrC contributes substantially to the total absorption. The contributions of coating-induced enhancements and of BrC are discussed further in Sections 3.4.1 and 3.4.2. The larger range of [OA]/[BC] and the greater number of individual burns considered here, compared to Pokhrel et al. (2016), allows for determination of more robust fits. Pokhrel et al. (2017) found that the absorption

enhancement at 405 nm, determined from thermodenuder measurements, increased with [OA]/[BC] up to [OA]/[BC] ~33 (the largest value reported), consistent with our findings.

These observations demonstrate that the optical properties of the primary particles depend on the relative amount of OA versus BC. This is as expected because OA is generally more scattering, compared to BC, and light absorbing OA (aka BrC) typically exhibits a much stronger wavelength dependence than BC. Based on these relationships, we divide the individual burns into different classes (**Table 1**). We have chosen to classify particles based on the observed SSA_{405nm} values; use of [OA]/[BC] for classification yields largely similar results, given the strong relationship between the two. The dividing lines between classes are selected to yield six classes that span the entire range of SSA_{405nm} values, from 0.23 (Class 1) to 0.97 (Class 6), with approximately equal numbers of individual burns in each class (ca. 8-10). Partitioning the observations into different particle classes facilitates interpretation of the photochemical evolution of the particles, to be discussed in future work. In addition, we find that use of the Class average properties versus MCE generally provides more representative fits to the observations (visually apparent in **Figure 1**, and supported by the reduced χ^2 for the fits).

3.2 OA composition and volatility

Variability in the bulk composition of the OA is characterized by the O:C and H:C atomic ratios and the fractional abundance (f_x) of two marker ions, m/z = 44 and m/z = 60. The f_{44} is complementary to O:C and larger values generally indicate a greater degree of oxygenation and the presence of carboxylic acids. The f_{60} is often taken as a marker ion for biomass burning, in particular a signature of levoglucosan and similar molecules (Schneider et al., 2006;Alfarra et al., 2007). The high resolution ion $C_2H_4O_2^+$ contributes to and exhibits similar behavior as f_{60}; the slope for $f_{C2H4O2+}$ against f_{60} is 0.98. While it is known that properties such as f_{60} vary in different biomass burning samples (Schneider et al., 2006) or between near-source intercepts of different ambient plumes (Garofalo et al., 2019), the specific dependence on burn conditions or overall particle composition (e.g. [OA]/[BC]) has not been systematically explored to our knowledge.

The average f_{60} = 0.022 ± 0.01 (1σ). The f_{60} values vary non-monotonically with [OA]/[BC], exhibiting a slight increase from Class 1 to Class 3 and then a decrease from Class 4 to Class 6 (Figure 2a). This indicates that, while f_{60} is overall a useful marker ion for biomass burning, it

cannot be used to distinguish between different burn conditions. The f_{44} generally decreases with [OA]/[BC] (Figure 2b; r^2 = 0.33.) However, the average f_{44} values for particle Classes 2-5 differ negligibly, suggesting that f_{44} might be useful in discriminating between extreme cases (e.g. Class 1 versus Class 6), but that it is of limited general use in distinguishing between burn conditions and fuel types. The O:C atomic ratio (average = 0.37 ± 0.09) exhibits similar behavior—expected as f_{44} is generally related to O:C (Aiken et al., 2008)—with a general decrease as [OA]/[BC] increases, although a comparably weaker correlation (Figure 2c; r^2 = 0.17). The H:C (average = 1.76 ± 0.05) exhibits a weak, positive correlation with [OA]/[BC], although the variability is slight (Figure 2d; r^2 = 0.27).

The mass fraction of the OA that is composed of nitrated organics ($f_{ON\text{-}OA}$ = [ON]/[OA]) was determined using the HR-ToF-AMS measurements and the method of Kiendler-Scharr et al. (2016) (see the Supplemental Material for further details). The terminology nitrated organics (ON) includes contributions from both nitro and nitrate functional groups. The fraction of measured nitrate that was ON ($f_{ON\text{-}N}$ = [ON]/([ON]+[NO_3^-]) decreased with [OA]/[BC] and ranged from 0.91 (Class 1) to 0.48 (Class 6) (**Figure S2a)**. The Class-specific average $f_{ON\text{-}OA}$ also decreased with [OA]/[BC], although by a much greater extent than the $f_{ON\text{-}N}$, ranging from 6.0% (Class 1) to 0.27% (Class 6) and (**Figure 2e**). There is a reasonably linear relationship between log($f_{ON\text{-}OA}$) and log([OA]/[BC]) (r^2 = 0.47). This indicates that a larger proportion of ON species and functionalities are produced when particles are, on average, more BC-rich. This does not reflect differences in fuel nitrogen content as there is no relationship between fuel N and $f_{ON\text{-}OA}$ (**Figure S2b**). Therefore, it seems that the relationship between $f_{ON\text{-}OA}$ and [OA]/[BC] is related more so to the burn conditions than the fuel N content, although as with many other properties the relationship with [OA]/[BC] is clearer than with the MCE (**Figure S2**c).

The OA volatility is characterized as the ratio between the OA concentration after thermodenuding to that without thermodenuding (the mass fraction remaining, MFR_{OA}). The MFR_{OA} decreases as [OA]/[BC] increases (**Figure 2f**), indicating that the OA at lower [OA]/[BC] is less volatile than the OA at higher values. This observation provides support for the proposal by Saleh et al. (2014) that less volatile, more absorbing species are preferentially formed under conditions where BC formation is favored, discussed further in Section 3.4.2. The relationship between MFR_{OA} and [OA]/[BC] is reasonably described by an exponential function.

3.3 BC Mixing State

As discussed above, the relative amounts of OA and BC vary greatly between fuel types and combustion conditions. However, the distribution of BC and OA between particles, and how this varies between very different burn conditions, has not been previously explored in detail to our knowledge. The bulk average fraction of OA that is internally mixed with BC versus OA that is externally mixed from BC is determined using the HR-ToF-AMS and SP-AMS measurements. The HR-ToF-AMS quantifies OA independent of mixing state, whereas the SP-AMS (as operated here) quantifies only the OA that is internally mixed with BC. The fraction of OA that is internally mixed with BC ($f_{OA,int}$) is:

$$f_{OA,int} = \frac{[OA]_{SP-AMS}}{[OA]_{HR-ToF-AMS}} = \frac{[OA]_{int}}{[OA]_{tot}} \quad (5)$$

where the subscript *int* indicates the OA that is internally mixed with BC and the subscript *tot* indicates the total OA. The $f_{OA,int}$ should range from 0 to 1. Related, the SP-AMS quantified the ratio between the OA that is internally mixed with BC and the BC concentration, referred to here as $[OA]_{int}/[BC]$. We find that $f_{OA,int}$ decreases substantially as [OA]/[BC] increases, ranging from $f_{OA,int} = 0.4$ for Class 1 (low SSA) particles to $f_{OA,int} = 0.01$ for Class 6 (high SSA) particles (**Figure 3a**). The data are well-fit by a sigmoidal function. However, the amount of OA coating BC ($R_{OA\text{-}BC} = [OA]_{int}/[BC]$) increases with the total [OA]/[BC], also with a sigmoidal relationship (**Figure 3b**). Thus, while a smaller fraction of the total OA is internally mixed with BC for larger total [OA]/[BC] the amount of OA that coats BC increases. Most likely this behavior reflects that BC and OA are generated with different efficiencies in different parts of the combusting biomass. BC is more efficiently generated from flaming combustion while OA is more efficiently generated from smoldering combustion. These observations demonstrate that the extent to which atmospheric models can assume that all OA is internally mixed with or externally mixed from BC at the point of emission will depend on the combustion conditions.

3.4 Absorption enhancement and brown carbon

3.4.1 Coating-induced absorption enhancement

Non- or weakly-absorbing coatings on black carbon particles can theoretically increase the absorption by BC (Fuller et al., 1999;Bond et al., 2006), an effect which has been confirmed by

laboratory experiments (Lack et al., 2009;Shiraiwa et al., 2010;Cappa et al., 2012). The extent to which coatings on BC actually enhance absorption by BC in the atmosphere remains unclear. Some studies indicate minor coating-induced enhancements while others indicate substantial enhancements (Cappa et al., 2012;Healy et al., 2015;Liu et al., 2015;Peng et al., 2016;Zhang et al., 2016;Liu et al., 2017;Cappa et al., 2019b). Understanding the nature of the coating-induced enhancement is important for quantifying the radiative impacts of BC (Jacobson, 2001;Bond et al., 2013). Further, these coating-induced absorption enhancements ($E_{abs.coat}$) complicate the determination of brown carbon (BrC) absorption and the two must be separated. Here, we examine the extent to which coatings on BC for primary biomass burning particles enhance the BC absorption. Theoretically, the magnitude of $E_{abs,coat}$ for an individual particle depends primarily on the coating thickness and secondarily on the size of the BC core (Bond et al., 2006; Fuller et al., 1999). Thus, the extent to which coatings enhance BC absorption for a given situation can be assessed through the relationship between the observed MAC_{BC} and the coating-to-core mass ratio ($R_{coat\text{-}rBC}$ = [NR-PM]$_{int}$/[BC], where *int* indicates that the coating material is internally mixed with BC). The expectation is that the MAC_{BC} increases with $R_{coat\text{-}BC}$.

However, absorption by BrC can also lead to an apparent increase in the normalized absorption with R_{BC} if the BrC abundance correlates with the total coating amount. Because BrC absorbs more strongly at shorter wavelengths, the wavelength-dependence of the MAC_{BC} to R_{BC} relationship can be used to further separate the influence of coating versus BrC absorption. The MAC_{BC} exhibits a wavelength-dependent relationship with $R_{coat\text{-}rBC}$ for fresh biomass particles (405 nm, 532 nm and 781 nm) (**Figure 4a-c**). The MAC_{BC} increases notably with $R_{coat\text{-}rBC}$ at 405 nm and to a lesser extent at 532 nm. At 781 nm the MAC_{BC} is essentially independent of $R_{coat\text{-}rBC}$ up to $R_{coat\text{-}rBC}$ values as large as 10, but does exhibit some increase at $R_{coat\text{-}rBC} > 10$. However, this is most likely a result of absorption by OA at 781 nm and not indicative of an increase in the coating-induced enhancement, discussed further below. The wavelength dependence provides clear evidence of BrC absorption at shorter wavelengths.

That the MAC_{BC} at 781 nm is nearly independent of $R_{coat\text{-}rBC}$ up to such large $R_{coat\text{-}rBC}$ values indicates that there is only a minor coating-induced enhancement for the primary biomass particles, the magnitude of which is discussed below. Our observations are consistent with McMeeking et al. (2014), who also investigated the relationship between the MAC_{BC} and $R_{coat\text{-}rBC}$ for a primary biomass particles from multiple fuel types. Most likely, this lack of a substantial coating-induced

enhancement results from a non-even distribution of non-BC mass across the population of BC particles (Fierce et al., 2016;Liu et al., 2017) and from the morphology of BC-containing particles not conforming to an idealized core-shell structure (Adachi et al., 2010). The influence of photochemical aging on the coating-induced enhancement will be examined in future work.

The relationship between MAC_{BC} and the coating amount ($R_{coat\text{-}rBC}$) can be contrasted with the relationship between MAC_{BC} and the total [OA]/[BC]. At all three wavelengths the MAC_{BC} exhibit strong, sigmoidal relationships with [OA]/[BC] (**Figure 4d-f**). That $MAC_{BC,781nm}$ exhibits such a clear relationship with [OA]/[BC] suggests that even the small apparent coating-induced enhancement, implied above from the very weak with $R_{coat\text{-}rBC}$, is largely driven by absorption by BrC rather than from the impact of coating on BC. Pokhrel et al. (2017) found that the absorption enhancement, determined from thermodenuder measurements, increased notably with [OA]/[BC] up to [OA]/[BC] ~33 at 405 nm (the largest value reported by them), but by much less at 660 nm, consistent with our findings.

The observations allow for determination of wavelength-dependent MAC_{BC} values for pure BC ($MAC_{BC,pure}$) for each wavelength by extrapolation of the MAC_{BC} versus [OA]/[BC] ratio to zero using sigmoid fits. Since the $R_{coat\text{-}rBC}$ correlates reasonably with [OA]/[BC] (**Figure 3**b), extrapolation against [OA]/[BC] to zero effectively removes both contributions from BrC and any coating-induced enhancement. The derived $MAC_{BC,pure}$ values are 11.8 $m^2\ g^{-1}$ at 405 nm, 8.8 $m^2\ g^{-1}$ at 532 nm and 5.5 $m^2\ g^{-1}$ at 781 nm, with estimated fit-based uncertainties of ~10%. The absolute uncertainties on the $MAC_{BC,pure}$ are primarily dependent on the uncertainty in the b_{abs} and [rBC] measurements, and are ~35%. The derived MAC_{BC} values are very similar to those recently reported by Forestieri et al. (2018) for fresh BC particles: $MAC_{BC,pure}$ = 11.9 $m^2\ g^{-1}$ at 405 nm and 8.8 $m^2\ g^{-1}$ at 532 nm, with an extrapolated value at 781 nm of 5.7 $m^2\ g^{-1}$. The value at 532 nm is somewhat higher than that suggested by Bond and Bergstrom (2006) (7.75 $m^2\ g^{-1}$ at 532 nm). Our derived $MAC_{BC,pure}$ values yield an AAE = 1.17, determined from a fit to the three wavelengths. An AAE close to unity indicates absorption is dominated by BC, as expected.

Values for the absorption enhancement at 781 nm are calculated as the ratio between the observed MAC_{BC} in **Figure 4** and the derived $MAC_{BC,pure}$. The derived E_{abs} range from 0.96 to 27. Values greater than two occur only for the particles having particularly large [OA]/[BC], > 400. As E_{abs} values much greater than two at 781 nm are unlikely to result from mixing-induced

enhancements (Chakrabarty and Heinson, 2018), this again suggests that the OA is somewhat absorbing at this wavelength. For the burns where [OA]/[BC] < 400, the median E_{abs} = 1.14 and the arithmetic mean E_{abs} = 1.19 ± 0.14 (1σ). Given that some of this enhancement may result from BrC absorption at 781, these values can be considered upper-limits on $E_{abs,coat}$, and the small magnitude is consistent with our conclusion above that, while likely greater than zero, the mixing-induced enhancement is generally minor. It is possible that the $E_{abs,coat}$ values when [OA]/[BC] > 400 are substantially larger. However, given the general lack of a dependence of the $MAC_{BC,781nm}$ for $R_{BC\text{-}coat}$ < 10 this seems unlikely.

3.4.2 Primary brown carbon absorption

The absorption due to brown carbon is determined by difference as:

$$\boldsymbol{b_{abs,BrC} = b_{abs,obs} - MAC_{BC,pure} \cdot [BC] \cdot E_{abs,coat}} \quad \textbf{(6)}$$

where $b_{abs,BrC}$ is the absorption due to BrC specifically. Importantly, the use of study-specific $MAC_{BC,pure}$ values serves to reduce systematic biases in the $b_{abs,BrC}$, compared to direct use of literature $MAC_{BC,pure}$ values. Assuming $E_{abs,coat}$ = 1 provides an upper limit on the BrC absorption, which we note is likely most appropriate for the particles sampled here, as discussed in the previous section. Therefore, we use the upper-limit values throughout the analysis that follows, unless otherwise stated. However, a lower limit for BrC absorption can be determined at 405 nm and 532 nm assuming that all of the enhancement at 781 nm results from coatings and not from BrC. The resulting $E_{abs,obs}$ (= $MAC_{BC,obs}/MAC_{BC,pure}$) at 781 nm averages 1.19 for $R_{BC\text{-}coat}$ < 10. Using $E_{abs,coat}$ = 1.19 in Eqn. 7 yields a lower limit for the BrC absorption at the two shorter wavelengths, appropriate since $E_{abs,coat}$ generally has only a small wavelength dependence. A fit to the coating-corrected (lower-limit) versus upper-limit $b_{abs,BrC}$ yields a slope of 0.97 at 405 nm and 0.88 at 532 nm (**Figure S3**). The smaller difference at 405 nm results from the fractional contribution of BrC to the total absorption being larger at this wavelength.

Brown carbon-specific mass absorption coefficients (MAC_{BrC}) are determined as the ratio between $b_{abs,BrC}$ and the total OA concentration:

$$\boldsymbol{MAC_{BrC} = \frac{b_{abs,BrC}}{[OA]}} \quad (7)$$

The MAC_{BrC} values from Eqn. **7** are bulk-average values, and do not account for different molecules and classes of molecules likely having different absorptivities. Uncertainties in the MAC_{BrC} values are determined by error propagation. Similarly, an AAE value for just the brown carbon (AAE_{BrC}) can be calculated using wavelength pairs as:

$$\boldsymbol{AAE_{BrC}} = -\mathbf{log}\left(\frac{\boldsymbol{b_{abs,BrC,\lambda_1}}}{\boldsymbol{b_{abs,BrC,\lambda_2}}}\right)/\mathbf{log}\left(\frac{\boldsymbol{\lambda_1}}{\boldsymbol{\lambda_2}}\right); \quad (8)$$

The geometric averages of the MAC_{BrC} values are $0.76^{+0.65}_{-0.35}$ m^2 g^{-1}, $0.21^{+0.36}_{-0.13}$ m^2 g^{-1}, $0.056^{+0.15}_{-0.04}$ m^2 g^{-1} at 405 nm, 532 nm and 781 nm, with uncertainties the 1σ burn-to-burn variability. The MAC_{BrC} values vary between classes, generally increasing as the [OA]/[BC] ratio decreases at all wavelengths (shown for 405 nm in **Figure 5**a). For example, the average MAC_{405nm} = 2.3 ± 1 m^2 g^{-1} for Class 1 and 0.35 ± 0.09 m^2 g^{-1} for Class 6. Although the uncertainties on the derived MAC_{BrC} increase substantially as [OA]/[BC] decreases—because BrC absorption contributes to a smaller extent at longer wavelengths—the observations nonetheless indicate that the BrC absorptivity depends on the combustion conditions. The relationship at 405 nm is well-described by a sigmoidal function in log-log space, with limiting values of 0.35 m^2 g^{-1} at large [OA]/[BC] and 11.2 m^2 g^{-1} at small [OA]/[BC]. That the extrapolated zero [OA]/[BC] limit for MAC_{BrC} is similar to pure BC suggests an evolution of BrC towards having properties similar to BC when the overall [OA] content is small. Such behavior is consistent with Saleh et al. (2018), who argue that there is a continuum of BrC properties that depends on the combustion conditions, as demonstrated in that study for low-temperature benzene and toluene combustion. The range of the MAC_{BrC} values observed here, including that there is notable absorption at 781 nm, encompass many previous measurements, summarized in **Table S3**. This likely reflects the wide diversity of fuel types and burn conditions considered here, as exemplified by the very large range of [OA]/[BC].

Estimated values of the imaginary component of the refractive index for BrC (k_{BrC}) are determined from Mie theory via optical closure (Zhang et al., 2016), assuming a real part of the refractive index of 1.5 and a particle diameter of 150 nm, a typical value for these experiments. Imaginary RI values are of use in atmospheric models for calculation of BrC absorption. There is a linear relationship between MAC_{BrC} and k_{BrC} (**Figure S4**a). Thus, the k_{BrC} exhibits a similar correlation with [OA]/[BC] as does the MAC_{BrC} (**Figure 5**a).

The wavelength-dependence of absorption, i.e. the $AAE_{405\text{-}532}$, also varies with [OA]/[BC], in this case with a positive relationship between the two (**Figure 5**b). The relationship is reasonably described by a sigmoidal function. This implies that, while the MAC_{BrC} varies inversely with [OA]/[BC] at all wavelengths, the exact variation is wavelength dependent. The $AAE_{405\text{-}532}$ relationship with [OA]/[BC] is well-described by a sigmoidal function (versus log([OA]/[BC]), with limiting values of 10.4 at large [OA]/[BC] and 1.3 at small [OA]/[BC]. The wavelength-dependence of the k_{BrC} (w_{BrC}) are also calculated, to facilitate comparison with the literature, as:

$$\boldsymbol{w_{BrC} = -\log\left(\frac{k_{BrC,\lambda 1}}{k_{BrC,\lambda 2}}\right) / \log\left(\frac{\lambda 1}{\lambda 2}\right)} \quad (9)$$

The w_{BrC} exhibit a similar dependence on [OA]/[BC] as the AAE_{BrC}, as the w_{BrC} and AAE_{BrC} are linearly related, albeit with some scatter (**Figure S4**b; $r^2 = 0.97$).

Our observations support the results of Saleh et al. (2014), who also found a relationship between the $k_{BrC,405nm}$ and [OA]/[BC]. However, our analysis substantially extends the range of [OA]/[BC] values investigated in that work (they considered [OA]/[BC] from only ca. 2 to 170). In the overlap region between our two studies the $k_{BrC,405nm}$ agree reasonably well over the range $2 < [OA]/[BC] < 50$, but the $k_{BrC,405nm}$ from Saleh et al. (2014) are smaller than observed here above [OA]/[BC] = 50. Importantly, our results demonstrate that the linear fit suggested by Saleh et al. (2014) for MAC_{BrC} is only appropriate over the range of values they considered and that a sigmoidal provides for a more robust relationship over a wider range of [OA]/[BC]. Related, the wider range of [OA]/[BC] enables more robust determination of the functional dependence of the wavelength-dependence of absorption (w_{BrC}), with overall larger w_{BrC} values and a larger plateau at high [OA]/[BC] compared to the fit by Saleh et al. (2014).

The MAC_{BrC} values also correlate with the nitrated organic fraction of OA, the latter of which, as noted above, also correlates with the [OA]/[BC] (**Figure 6**a). This observation suggests that organic nitrate and nitro functionalities may be at least somewhat responsible for the increase in absorption. Laskin et al. (2018) performed offline molecular level analyses of primary OA collected during FIREX. They found that nitroaromatics and N-containing polycyclic aromatic hydrocarbons (PAHs) contribute notably to the total light absorption by BrC, although there are many non-N-containing species that also contribute to BrC absorption. The variability between particle Classes is consistent with the results of Lin et al. (2016), which show that the abundance

of N-containing chromophores varies between particles produced from different biomass fuels. Additionally Mohr et al. (2013) observed a relationship between the concentration of nitrated phenols and short-wavelength absorption by BrC, although it is possible that for their measurements these species were produced from chemical processing, as opposed to being directly emitted. Altogether, our results provide support for the idea that nitrated organic functionalities are an important contributor to BrC absorption. However, it is very likely that other functional groups also contribute to the total absorption.

The $MAC_{BrC,405nm}$ exhibits an inverse correlation with the f_{60}/f_{44} ratio of the OA, although there is substantial scatter in the f_{60}/f_{44} ratio for a given particle class (**Figure 6**b). (The f_{44} and f_{60} have no discernable relationship.) The observed $MAC_{BrC,405nm}$ relationship with f_{60}/f_{44} is opposite that reported by Lack et al. (2013) for ambient measurements of particles a biomass burning plume, who find a reasonable positive correlation. This difference in behavior results from our sampling primary particles directly—thereby focusing on the inherent variability in the properties of the emitted particles—while Lack et al. (2013) sampled ambient particles. For ambient sampling, the observed relationship will be sensitive to mixing of biomass burning particles with background or aged biomass particles, which are known to have a smaller f_{60} (Cubison et al., 2011). Thus, the relationship observed by Lack et al. (2013) can best be viewed as a mixing line between the fresh primary particles (having large $MAC_{BrC,405nm}$ and large f_{60}/f_{44}) and background or aged biomass particles (having small $MAC_{BrC,405nm}$ and small f_{60}/f_{44}), rather than providing information on the inherent variability in the absorptivity of the fresh particles.

3.5 Size distributions

Total particle mobility size distributions and BC-only size distributions were measured (**Figure 7**). Primary particle size distributions are important parameters specified in regional and global models. The number-weighted and volume-weighted size distributionare generally described by either one or two log-normal modes for individual burns; a two-mode fit provides a more robust solution across all modes. The mass-weighted BC size distributions are similarly described by one or two log-normal modes. A fit to the average number-weighted distribution across all particle classes yields geometric median diameters ($d_{p,N}$) and widths (σ_g) of 60.3 nm and 1.76, respectively, for the smaller mode and 153 nm and 1.64 for the larger mode (**Figure 8**). The amplitude of the smaller mode is 4.6 times the larger mode. A single mode fit yields $d_{p,N}$ = 68 nm and χ_g = 1.93,

438 although the fit is poorer. Mann et al. (2014) report $d_{p,N}$ values used by a variety of global models
439 for biofuels. The models tend to use either 80 nm or 150 nm, although a few use other values (30
440 nm, 60 nm, 100 nm). Those using 80 nm typically use $\sigma_g = 1.80$ while those using 150 nm typically
441 use $\sigma_g = 1.59$, although there are exceptions. Our observations indicate that use of a bimodal
442 distribution within models would be more representative, but that a single mode can do acceptably.
443 We find that the volume-weighted distribution calculated from a single-mode fit to the number-
444 weighted distribution is similar to the observed volume-weighted distribution (**Figure 8**). Thus,
445 the use of a single-mode to represent biomass burning size distributions thus appears acceptable,
446 so long as the appropriate parameters are used. In this context, the widths of the distribution used
447 by the various global models appear somewhat too small. However, we note that the microphysics
448 occurring in the fresh smoke sampled here, which will govern the size distributions, may differ
449 from that in atmospheric plumes.

450 The average BC-specific mass-weighted size distribution mode is at 148 nm (**Figure 8**). A
451 bimodal fit yields values for the mass median diameter ($d_{p,M}$) and σ_g of 137.2 nm and 1.62,
452 respectively, for the smaller mode and 197.1 nm and 1.24 for the larger mode, with most of the
453 mass contained in the smaller mode. May et al. (2014) report $d_{p,M}$ from laboratory biomass
454 combustion ranging from 140-190 nm, averaging 170 nm. Their average is somewhat larger than
455 ours, likely reflecting differences in the exact fuels sampled. The mode diameter for the BC-
456 specific distribution is especially smaller than observed for biomass burning particles from some
457 ambient observations, which tend to give values closer to 200 nm (Schwarz et al., 2008;Kondo et
458 al., 2011;Sahu et al., 2012;May et al., 2014;Cappa et al., 2019b). This difference between lab and
459 field observations was also noted by May et al. (2014). We speculate that the influence of
460 coagulation may be suppressed in our experiments relative to what occurs in the atmosphere due
461 to slower overall dilution, leading to smaller BC size distributions. To the extent this is the reason
462 for the difference, the total particle distributions would also be biased towards too small particles,
463 compared to the atmosphere. However, there is no relationship between $d_{p,N}$ and the total particle
464 number concentration for our experiments. Formation of secondary aerosol in the near-field of a
465 sampled ambient plume could also contribute to this difference.

466 There is substantial variability between individual burns within a given particle Class in terms
467 of the shape of the size distributions (**Figure 7**). This variability is most evident for Class 1, 2 and

5, but present for all Classes. Nonetheless, the number-weighted mean diameter ($d_{p,N,mean}$) appears to decrease somewhat with MCE (**Figure 9**; $r^2 = 0.38$). However, the relationship is largely driven by the Class 6 particles, which generally have lower MCE values, having larger $d_{p,N,mean}$ values. A lack of any particularly clear relationship is consistent with Hosseini et al. (2010), who observed the $d_{p,N,mean}$ to exhibit a complex relationship with combustion conditions. The $d_{p,N,mean}$ varies non-monotonically with [OA]/[BC], with particle size first decreasing slightly as [OA]/[BC] increases (from Class 1 to Class 3) and then increasing with further increases in [OA]/[BC] (from Class 4 to Class 6) (**Figure 9**). This is despite the notable burn-to-burn variability. It is important to note that the mobility-based size is particle shape-dependent; very BC-rich particles are more likely to have non-spherical shapes and thus have larger mobility diameters. This could explain the minimum in $d_{p,N}$ around Class 3 particles, for which [OA]/[BC] = 10.

Some of the variability within a class appears related to the presence of different fuel types within a class. Number-weighted and BC-specific mass-weighted size distributions by fuel type are shown in **Figure 10**. For the number-weighted distributions, leaf litter and rotten logs exhibit the greatest variability between different burns, although we note that multiple burns were not performed for all fuels. The shapes of the leaf litter, peat and "other" fuel types differ most notably from the other fuel types, with the presence of more than one mode more apparent. (The "other" category here includes non-traditional biofuels, specifically building materials and excelsior.) For the BC-specific size distributions, the litter, canopy, and duff exhibited the greatest intra-fuel variability. For most fuels, the BC-specific distribution peaks around 150 nm, as noted above. However, for a subset of burns (eight of them) the BC-specific distribution peaks around 100 nm (**Figure 10**). These small BC-mode distributions occur for the OA-rich particle classes 4, 5 and 6 (**Figure 7**), although there is no clear pattern to their occurrence.

4 Conclusions and Implications

Measurements of primary particles produced from combustion of a variety of biomass fuel types indicate the optical, physical, and chemical properties of the emitted particles exhibit wide variability. We show that variability in many optical properties (e.g. single scatter albedo, wavelength dependence of absorption, mass absorptivity of black and brown carbon) is directly linked to the [OA]/[BC] ratio of the emitted particles; the relationships with [OA]/[BC] are much stronger than with the commonly used modified combustion efficiency, and mathematical

relationships between the various properties are determined. However, the absorption enhancement due to coating of BC (the so-called "lensing" effect) is shown to be minor and essentially independent of the amount of coating up to large coating-to-BC mass ratios. The brown carbon mass absorptivity correlates with the nitrated organic fraction of OA, suggesting that nitrated organic species contribute to BrC absorption. Many bulk chemical properties (i.e. O:C, H:C, and the relative concentrations of key marker ions such as f_{60}) exhibit limited dependence on the burn conditions and the [OA]/[BC] ratio. However, both the OA volatility and nitrated organic fraction of OA decrease with [OA]/[BC]. The fraction of OA that is internally mixed with BC was shown to decrease strongly with the [OA]/[BC] ratio, from nearly all OA being internally mixed with BC when the particles are overall BC-rich to only a few percent of OA being mixed with BC when OA dominates. Yet, the relative amount of OA coating the BC increases with [OA]/[BC]; that is, when more of the OA is externally mixed from BC those particles that do contain BC nonetheless have thicker OA coatings. The observed total particle size distributions are reasonably well described by a single log-normal mode, but are better fit using a bimodal distribution. The BC-specific size distributions are similarly best fit using a bimodal distribution, although a single mode provides a reasonable representation. The dependence of the geometric median mobility diameter on the burn conditions or particle state (i.e. the [OA]/[BC]) is complicated by the mobility diameter being sensitive to variations in particle shape, which depend on the [OA]/[BC] ratio. Overall, these results expand on previous observations of primary biomass burning particle properties, considering a wider range of [OA]/[BC] and associated properties. Further, they provide a foundation for understanding the post-emission evolution of biomass burning smoke due to photochemical oxidation as discussed in Lim et al. (2019).

5 Data Availability

All data are available from the NOAA FIREX-AQ data repository (https://esrl.noaa.gov/csd/projects/firex/firelab/). This includes a summary of the fuel types used for each burn and the measurement time-series for each burn. The primary particle averages used in this work are additionally collected in the UC DASH data repository (Cappa et al., 2019a).

6 Author Contributions

CDC and JHK designed the experiments. CDC, CYL, and DHH carried out the measurements and data processing. CDC, CDM, and CYL analyzed data. CDC and CDM wrote the manuscript, with contributions from all co-authors.

7 Acknowledgements

This work was supported by the National Oceanic and Atmospheric Administration Atmospheric Chemistry, Carbon Cycle & Climate Program, awards NA16OAR4310111 and NA16OAR4310112. CYL was additionally supported by the National Science Foundation Graduate Research Fellowship Program. The entire FIREX team, especially Bob Yokelson and Jim Roberts and the staff of the Missoula Fire Sciences Laboratory, are acknowledged for their assistance. Putting together the community inlet was a community effort—thank you to all who contributed. Shuka Schwarz and Gavin McMeeking are also thanked for their assistance with the SP2.

8 References

Adachi, K., Chung, S. H., and Buseck, P. R.: Shapes of soot aerosol particles and implications for their effects on climate, J. Geophys. Res., 115, D15206, https://doi.org/10.1029/2009jd012868, 2010.

Adler, G., Flores, J. M., Abo Riziq, A., Borrmann, S., and Rudich, Y.: Chemical, physical, and optical evolution of biomass burning aerosols: a case study, Atmos. Chem. Phys., 11, 1491-1503, https://doi.org/10.5194/acp-11-1491-2011, 2011.

Aiken, A. C., Decarlo, P. F., Kroll, J. H., Worsnop, D. R., Huffman, J. A., Docherty, K. S., Ulbrich, I. M., Mohr, C., Kimmel, J. R., Sueper, D., Sun, Y., Zhang, Q., Trimborn, A., Northway, M., Ziemann, P. J., Canagaratna, M. R., Onasch, T. B., Alfarra, M. R., Prevot, A. S. H., Dommen, J., Duplissy, J., Metzger, A., Baltensperger, U., and Jimenez, J. L.: O/C and OM/OC ratios of primary, secondary, and ambient organic aerosols with high-resolution time-of-flight aerosol mass spectrometry, Environ. Sci. Technol., 42, 4478-4485, https://doi.org/10.1021/es703009q, 2008.

Alexander, D. T. L., Crozier, P. A., and Anderson, J. R.: Brown Carbon Spheres in East Asian Outflow and Their Optical Properties, Science, 321, 833-836, https://doi.org/10.1126/science.1155296, 2008.

Alfarra, M. R., Prevot, A. S. H., Szidat, S., Sandradewi, J., Weimer, S., Lanz, V. A., Schreiber, D., Mohr, M., and Baltensperger, U.: Identification of the Mass Spectral Signature of Organic Aerosols from Wood Burning Emissions, Environmental Science & Technology, 41, 5770-5777, https://doi.org/10.1021/es062289b, 2007.

Andreae, M. O., and Merlet, P.: Emission of trace gases and aerosols from biomass burning, Global Biogeochemical Cycles, 15, 955-966, https://doi.org/doi:10.1029/2000GB001382, 2001.

Bluvshtein, N., Lin, P., Flores, J. M., Segev, L., Mazar, Y., Tas, E., Snider, G., Weagle, C., Brown, S. S., Laskin, A., and Rudich, Y.: Broadband optical properties of biomass-burning aerosol and identification of brown carbon chromophores, Journal of Geophysical Research: Atmospheres, 122, 5441-5456, https://doi.org/doi:10.1002/2016JD026230, 2017.

Bond, T. C., and Bergstrom, R. W.: Light absorption by carbonaceous particles: An investigative review, Aerosol Science and Technology, 40, 27-67, https://doi.org/10.1080/02786820500421521, 2006.

Bond, T. C., Habib, G., and Bergstrom, R. W.: Limitations in the enhancement of visible light absorption due to mixing state, J. Geophys. Res.-Atmos., 111, https://doi.org/10.1029/2006JD007315, 2006.

Bond, T. C., Doherty, S. J., Fahey, D. W., Forster, P. M., Berntsen, T., DeAngelo, B. J., Flanner, M. G., Ghan, S., Kärcher, B., Koch, D., Kinne, S., Kondo, Y., Quinn, P. K., Sarofim, M. C., Schultz, M. G., Schulz, M., Venkataraman, C., Zhang, H., Zhang, S., Bellouin, N., Guttikunda, S. K., Hopke, P. K., Jacobson, M. Z., Kaiser, J. W., Klimont, Z., Lohmann, U., Schwarz, J. P., Shindell, D., Storelvmo, T., Warren, S. G., and Zender, C. S.: Bounding the role of black carbon in the climate system: A scientific assessment, Journal of Geophysical Research: Atmospheres, 118, 1-173, https://doi.org/10.1002/jgrd.50171, 2013.

Bruns, E. A., Perraud, V., Zelenyuk, A., Ezell, M. J., Johnson, S. N., Yu, Y., Imre, D., Finlayson-Pitts, B. J., and Alexander, M. L.: Comparison of FTIR and Particle Mass Spectrometry for the

579 Measurement of Particulate Organic Nitrates, Environmental Science & Technology, 44, 1056-
580 1061, https://doi.org/10.1021/es9029864, 2010.

581 Canagaratna, M. R., Jayne, J. T., Jimenez, J. L., Allan, J. D., Alfarra, M. R., Zhang, Q., Onasch,
582 T. B., Drewnick, F., Coe, H., Middlebrook, A., Delia, A., Williams, L. R., Trimborn, A. M.,
583 Northway, M. J., DeCarlo, P. F., Kolb, C. E., Davidovits, P., and Worsnop, D. R.: Chemical and
584 microphysical characterization of ambient aerosols with the Aerodyne aerosol mass spectrometer,
585 Mass Spectrometry Reviews, 26, 185-222, https://doi.org/10.1002/mas.20115, 2007.

586 Cappa, C. D., Onasch, T. B., Massoli, P., Worsnop, D., Bates, T. S., Cross, E., Davidovits, P.,
587 Hakala, J., Hayden, K., Jobson, B. T., Kolesar, K. R., Lack, D. A., Lerner, B., Li, S. M., Mellon,
588 D., Nuaanman, I., Olfert, J., Petaja, T., Quinn, P. K., Song, C., Subramanian, R., Williams, E. J.,
589 and Zaveri, R. A.: Radiative absorption enhancements due to the mixing state of atmospheric black
590 carbon, Science, 337, 1078-1081, https://doi.org/10.1126/science.1223447, 2012.

591 Cappa, C. D., Lim, C. Y., Hagan, D. H., and Kroll, J. H.: Measurements from the Fire Influence
592 on Regional and Global Environments Experiment (FIREX) Fire Lab Mini Chamber Experiment,
593 UC Davis DASH, Dataset, version 1, https://doi.org/10.25338/B8CK5N, 2019a.

594 Cappa, C. D., Zhang, X., Russell, L. M., Collier, S., Lee, A. K. Y., Chen, C.-L., Betha, R., Chen,
595 S., Liu, J., Price, D. J., Sanchez, K. J., McMeeking, G., Williams, L. R., Onasch, T. B., Worsnop,
596 D. R., Abbatt, J., and Zhang, Q.: Light absorption by ambient black and brown carbon and its
597 dependence on black carbon coating state for two California, USA cities in winter and summer,
598 Journal of Geophysical Research-Atmospheres, https://doi.org/10.1029/2018JD029501, 2019b.

599 Chakrabarty, R. K., Moosmüller, H., Chen, L. W. A., Lewis, K., Arnott, W. P., Mazzoleni, C.,
600 Dubey, M. K., Wold, C. E., Hao, W. M., and Kreidenweis, S. M.: Brown carbon in tar balls from
601 smoldering biomass combustion, Atmospheric Chemistry and Physics, 10, 6363-6370,
602 https://doi.org/10.5194/acp-10-6363-2010, 2010.

603 Chakrabarty, R. K., and Heinson, W. R.: Scaling Laws for Light Absorption Enhancement Due to
604 Nonrefractory Coating of Atmospheric Black Carbon Aerosol, Physical Review Letters, 121,
605 218701, https://doi.org/10.1103/PhysRevLett.121.218701, 2018.

606 Chen, Y., and Bond, T. C.: Light absorption by organic carbon from wood combustion, Atmos.
607 Chem. Phys., 10, 1773-1787, https://doi.org/10.5194/acp-10-1773-2010, 2010.

608 Coggon, M. M., Lim, C. Y., Koss, A. R., Sekimoto, K., Yuan, B., Cappa, C. D., Kroll, J. H.,
609 Selimovic, V., Zarzana, K. J., Brown, S. S., Roberts, J. M., Müller, M., Yokelson, R. J., Wisthaler,
610 A., Krechmer, J., Jimenez, J. L., De Gouw, J., and Warneke, C.: OH-chemistry of volatile organic
611 compounds emitted from laboratory and ambient biomass burning smoke: Influence of furans and
612 oxygenated aromatics on ozone and secondary VOC formation., Atmos. Chem. Phys. Discuss.,
613 https://doi.org/10.5194/acp-2019-516, 2019.

614 Collier, S., Williams, L. R., Onasch, T. B., Cappa, C. D., Zhang, X., Russell, L. M., Chen, C.-L.,
615 Sanchez, K. J., Worsnop, D. R., and Zhang, Q.: Influence of emissions and aqueous processing on
616 particles containing black carbon in a polluted urban environment: Insights from a soot particle –
617 aerosol mass spectrometer, Journal of Geophysical Research-Atmospheres, *123*, 6648-6666,
618 https://doi.org/10.1002/2017JD027851, 2018.

619 Cubison, M. J., Ortega, A. M., Hayes, P. L., Farmer, D. K., Day, D., Lechner, M. J., Brune, W. H.,
620 Apel, E., Diskin, G. S., Fisher, J. A., Fuelberg, H. E., Hecobian, A., Knapp, D. J., Mikoviny, T.,

621 Riemer, D., Sachse, G. W., Sessions, W., Weber, R. J., Weinheimer, A. J., Wisthaler, A., and
622 Jimenez, J. L.: Effects of aging on organic aerosol from open biomass burning smoke in aircraft
623 and laboratory studies, Atmos. Chem. Phys., 11, 12049-12064, https://doi.org/10.5194/acp-11-
624 12049-2011, 2011.

625 Fierce, L., Bond, T. C., Bauer, S. E., Mena, F., and Riemer, N.: Black carbon absorption at the
626 global scale is affected by particle-scale diversity in composition, Nat. Comm., 7,
627 https://doi.org/10.1038/ncomms12361, 2016.

628 Forestieri, S. D., Helgestad, T. M., Lambe, A. T., Renbaum-Wolff, L. H., Lack, D. A., Massoli,
629 P., Cross, E. S., Dubey, M. K., Mazzoleni, C., Olfert, J., Freedman, A., Davidovits, P., Onasch, T.
630 B., and Cappa, C. D.: Measurement and modeling of the multi-wavelength optical properties of
631 uncoated flame-generated soot, Atmos. Chem. Phys., 18, 12141-12159,
632 https://doi.org/10.5194/acp-18-12141-2018, 2018.

633 Forrister, H., Liu, J., Scheuer, E., Dibb, J., Ziemba, L., Thornhill, K. L., Anderson, B., Diskin, G.,
634 Perring, A. E., Schwarz, J. P., Campuzano-Jost, P., Day, D. A., Palm, B. B., Jimenez, J. L., Nenes,
635 A., and Weber, R. J.: Evolution of brown carbon in wildfire plumes, Geophysical Research Letters,
636 42, 4623-4630, https://doi.org/10.1002/2015GL063897, 2015.

637 Fuller, K. A., Malm, W. C., and Kreidenweis, S. M.: Effects of mixing on extinction by
638 carbonaceous particles, J. Geophys. Res.-Atmos., 104, 15941-15954,
639 https://doi.org/10.1029/1998jd100069, 1999.

640 Garofalo, L. A., Pothier, M. A., Levin, E. J. T., Campos, T., Kreidenweis, S. M., and Farmer, D.
641 K.: Emission and Evolution of Submicron Organic Aerosol in Smoke from Wildfires in the
642 Western United States, ACS Earth and Space Chem., 3, 1237-1247,
643 https://doi.org/10.1021/acsearthspacechem.9b00125, 2019.

644 Healy, R., Wang, J., Jeong, C. H., Lee, A., Willis, M., Jaroudi, E., Zimmerman, N., Hilker, N.,
645 Murphy, M., and Eckhardt, S.: Light-absorbing properties of ambient black carbon and brown
646 carbon from fossil fuel and biomass burning sources, Journal of Geophysical Research:
647 Atmospheres, 120, 6619-6633, 2015.

648 Hoffer, A., Gelencser, A., Guyon, P., Kiss, G., Schmid, O., Frank, G. P., Artaxo, P., and Andreae,
649 M. O.: Optical properties of humic-like substances (HULIS) in biomass-burning aerosols,
650 Atmospheric Chemistry and Physics, 6, 3563-3570, 2006.

651 Hoffer, A., Tóth, A., Nyirő-Kósa, I., Pósfai, M., and Gelencsér, A.: Light absorption properties of
652 laboratory-generated tar ball particles, Atmos. Chem. Phys., 16, 239-246,
653 https://doi.org/10.5194/acp-16-239-2016, 2016.

654 Hosseini, S., Li, Q., Cocker, D., Weise, D., Miller, A., Shrivastava, M., Miller, J. W., Mahalingam,
655 S., Princevac, M., and Jung, H.: Particle size distributions from laboratory-scale biomass fires
656 using fast response instruments, Atmos. Chem. Phys., 10, 8065-8076, https://doi.org/10.5194/acp-
657 10-8065-2010, 2010.

658 Jacobson, M. Z.: Strong radiative heating due to the mixing state of black carbon in atmospheric
659 aerosols, Nature, 409, 695-697, https://doi.org/10.1038/35055518, 2001.

660 Jen, C. N., Hatch, L. E., Selimovic, V., Yokelson, R. J., Weber, R., Fernandez, A. E., Kreisberg,
661 N. M., Barsanti, K. C., and Goldstein, A. H.: Speciated and total emission factors of particulate

662 organics from burning western U.S. wildland fuels and their dependence on combustion efficiency,
663 Atmos. Chem. Phys., 19, 1013-1026, https://doi.org/10.5194/acp-19-1013-2019, 2019.

664 Kiendler-Scharr, A., Mensah, A. A., Friese, E., Topping, D., Nemitz, E., Prevot, A. S. H., Äijälä,
665 M., Allan, J., Canonaco, F., Canagaratna, M., Carbone, S., Crippa, M., Dall Osto, M., Day, D. A.,
666 De Carlo, P., Di Marco, C. F., Elbern, H., Eriksson, A., Freney, E., Hao, L., Herrmann, H.,
667 Hildebrandt, L., Hillamo, R., Jimenez, J. L., Laaksonen, A., McFiggans, G., Mohr, C., O'Dowd,
668 C., Otjes, R., Ovadnevaite, J., Pandis, S. N., Poulain, L., Schlag, P., Sellegri, K., Swietlicki, E.,
669 Tiitta, P., Vermeulen, A., Wahner, A., Worsnop, D., and Wu, H.-C.: Ubiquity of organic nitrates
670 from nighttime chemistry in the European submicron aerosol, Geophysical Research Letters, 43,
671 7735-7744, https://doi.org/doi:10.1002/2016GL069239, 2016.

672 Kirchstetter, T. W., Novakov, T., and Hobbs, P. V.: Evidence that the spectral dependence of light
673 absorption by aerosols is affected by organic carbon, Journal of Geophysical Research-
674 Atmospheres, 109, D21208, 2004.

675 Kondo, Y., Matsui, H., Moteki, N., Sahu, L., Takegawa, N., Kajino, M., Zhao, Y., Cubison, M. J.,
676 Jimenez, J. L., Vay, S., Diskin, G. S., Anderson, B., Wisthaler, A., Mikoviny, T., Fuelberg, H. E.,
677 Blake, D. R., Huey, G., Weinheimer, A. J., Knapp, D. J., and Brune, W. H.: Emissions of black
678 carbon, organic, and inorganic aerosols from biomass burning in North America and Asia in 2008,
679 J. Geophys. Res., 116, D08204, https://doi.org/10.1029/2010jd015152, 2011.

680 Koss, A. R., Sekimoto, K., Gilman, J. B., Selimovic, V., Coggon, M. M., Zarzana, K. J., Yuan, B.,
681 Lerner, B. M., Brown, S. S., Jimenez, J. L., Krechmer, J., Roberts, J. M., Warneke, C., Yokelson,
682 R. J., and de Gouw, J.: Non-methane organic gas emissions from biomass burning: identification,
683 quantification, and emission factors from PTR-ToF during the FIREX 2016 laboratory experiment,
684 Atmos. Chem. Phys., 18, 3299-3319, https://doi.org/10.5194/acp-18-3299-2018, 2018.

685 Lack, D. A., Cappa, C. D., Cross, E. S., Massoli, P., Ahern, A. T., Davidovits, P., and Onasch, T.
686 B.: Absorption Enhancement of Coated Absorbing Aerosols: Validation of the Photo-Acoustic
687 Technique for Measuring the Enhancement, Aerosol Science and Technology, 43, 1006-1012,
688 https://doi.org/10.1080/02786820903117932, 2009.

689 Lack, D. A., Langridge, J., Bahreni, R., Cappa, C. D., Middlebrook, A., and Schwarz, J. P.: Brown
690 Carbon and Internal Mixing in Biomass Burning Particles, PNAS, 10, 14802-14807,
691 https://doi.org/10.1073/pnas.1206575109, 2012a.

692 Lack, D. A., Richardson, M. S., Law, D., Langridge, J. M., Cappa, C. D., McLaughlin, R. J., and
693 Murphy, D. M.: Aircraft Instrument for Comprehensive Characterization of Aerosol Optical
694 Properties, Part 2: Black and Brown Carbon Absorption and Absorption Enhancement Measured
695 with Photo Acoustic Spectroscopy, Aerosol Science and Technology, 46, 555-568,
696 https://doi.org/10.1080/02786826.2011.645955, 2012b.

697 Lack, D. A., Bahreini, R., Langridge, J. M., Gilman, J. B., and Middlebrook, A. M.: Brown carbon
698 absorption linked to organic mass tracers in biomass burning particles, Atmos. Chem. Phys., 13,
699 2415-2422, https://doi.org/10.5194/acp-13-2415-2013, 2013.

700 Langridge, J. M., Richardson, M. S., Lack, D., Law, D., and Murphy, D. M.: Aircraft Instrument
701 for Comprehensive Characterization of Aerosol Optical Properties, Part I: Wavelength-Dependent
702 Optical Extinction and Its Relative Humidity Dependence Measured Using Cavity Ringdown
703 Spectroscopy, Aerosol Science and Technology, 45, 1305-1318,
704 https://doi.org/10.1080/02786826.2011.592745, 2011.

Laskin, A., Lin, P., Laskin, J., Fleming, L. T., and Nizkorodov, S.: Molecular Characterization of Atmospheric Brown Carbon, in: Multiphase Environmental Chemistry in the Atmosphere, ACS Symposium Series, 1299, American Chemical Society, 261-274, 2018.

Levin, E. J. T., McMeeking, G. R., Carrico, C. M., Mack, L. E., Kreidenweis, S. M., Wold, C. E., Moosmüller, H., Arnott, W. P., Hao, W. M., Collett, J. L., and Malm, W. C.: Biomass burning smoke aerosol properties measured during Fire Laboratory at Missoula Experiments (FLAME), Journal of Geophysical Research: Atmospheres, 115, D18210, https://doi.org/10.1029/2009JD013601, 2010.

Lim, C. Y., Hagan, D. H., Coggon, M. M., Koss, A. R., Sekimoto, K., De Gouw, J., Warneke, C., Cappa, C. D., and Kroll, J. H.: Secondary organic aerosol formation from biomass burning emissions, Atmos. Chem. Phys. Discuss., https://doi.org/10.5194/acp-2019-326, 2019.

Lin, P., Aiona, P. K., Li, Y., Shiraiwa, M., Laskin, J., Nizkorodov, S. A., and Laskin, A.: Molecular Characterization of Brown Carbon in Biomass Burning Aerosol Particles, Environmental Science & Technology, 50, 11815-11824, https://doi.org/10.1021/acs.est.6b03024, 2016.

Liu, D. T., Whitehead, J., Alfarra, M. R., Reyes-Villegas, E., Spracklen, D. V., Reddington, C. L., Kong, S. F., Williams, P. I., Ting, Y. C., Haslett, S., Taylor, J. W., Flynn, M. J., Morgan, W. T., McFiggans, G., Coe, H., and Allan, J. D.: Black-carbon absorption enhancement in the atmosphere determined by particle mixing state, Nat. Geosci., 10, 184-U132, https://doi.org/10.1038/ngeo2901, 2017.

Liu, S., Aiken, A. C., Arata, C., Dubey, M. K., Stockwell, C. E., Yokelson, R. J., Stone, E. A., Jayarathne, T., Robinson, A. L., DeMott, P. J., and Kreidenweis, S. M.: Aerosol single scattering albedo dependence on biomass combustion efficiency: Laboratory and field studies, Geophysical Research Letters, 2013GL058392, https://doi.org/10.1002/2013GL058392, 2013.

Liu, S., Aiken, A. C., Gorkowski, K., Dubey, M. K., Cappa, C. D., Williams, L. R., Herndon, S. C., Massoli, P., Fortner, E. C., Chhabra, P. S., Brooks, W. A., Onasch, T. B., Worsnop, D. R., China, S., Sharma, N., Mazzoleni, C., Xu, L., L., N. N., Liu, D., Allan, J. D., Lee, J. D., Fleming, Z. L., Mohr, C., Zotter, P., Szidat, S., and Prevot, A. S. H.: Enhanced light absorption by mixed source black and brown carbon particles in UK winter, Nat. Comm., 6, 8435, https://doi.org/10.1038/ncomms9435, 2015.

Mann, G. W., Carslaw, K. S., Reddington, C. L., Pringle, K. J., Schulz, M., Asmi, A., Spracklen, D. V., Ridley, D. A., Woodhouse, M. T., Lee, L. A., Zhang, K., Ghan, S. J., Easter, R. C., Liu, X., Stier, P., Lee, Y. H., Adams, P. J., Tost, H., Lelieveld, J., Bauer, S. E., Tsigaridis, K., van Noije, T. P. C., Strunk, A., Vignati, E., Bellouin, N., Dalvi, M., Johnson, C. E., Bergman, T., Kokkola, H., von Salzen, K., Yu, F., Luo, G., Petzold, A., Heintzenberg, J., Clarke, A., Ogren, J. A., Gras, J., Baltensperger, U., Kaminski, U., Jennings, S. G., O'Dowd, C. D., Harrison, R. M., Beddows, D. C. S., Kulmala, M., Viisanen, Y., Ulevicius, V., Mihalopoulos, N., Zdimal, V., Fiebig, M., Hansson, H. C., Swietlicki, E., and Henzing, J. S.: Intercomparison and evaluation of global aerosol microphysical properties among AeroCom models of a range of complexity, Atmos. Chem. Phys., 14, 4679-4713, https://doi.org/10.5194/acp-14-4679-2014, 2014.

May, A. A., McMeeking, G. R., Lee, T., Taylor, J. W., Craven, J. S., Burling, I., Sullivan, A. P., Akagi, S., Collett Jr., J. L., Flynn, M., Coe, H., Urbanski, S. P., Seinfeld, J. H., Yokelson, R. J., and Kreidenweis, S. M.: Aerosol emissions from prescribed fires in the United States: A synthesis

of laboratory and aircraft measurements, Journal of Geophysical Research: Atmospheres, 119, 11,826-811,849, https://doi.org/10.1002/2014JD021848, 2014.

McMeeking, G. R., Kreidenweis, S. M., Baker, S., Carrico, C. M., Chow, J. C., Collett, J. L., Hao, W. M., Holden, A. S., Kirchstetter, T. W., Malm, W. C., Moosmüller, H., Sullivan, A. P., and Wold, C. E.: Emissions of trace gases and aerosols during the open combustion of biomass in the laboratory, Journal of Geophysical Research: Atmospheres, 114, D19210, https://doi.org/10.1029/2009JD011836, 2009.

McMeeking, G. R., Fortner, E., Onasch, T. B., Taylor, J. W., Flynn, M., Coe, H., and Kreidenweis, S. M.: Impacts of nonrefractory material on light absorption by aerosols emitted from biomass burning, Journal of Geophysical Research: Atmospheres, 119, 12,272-212,286, https://doi.org/10.1002/2014JD021750, 2014.

Metcalf, A. R., Loza, C. L., Coggon, M. M., Craven, J. S., Jonsson, H. H., Flagan, R. C., and Seinfeld, J. H.: Secondary Organic Aerosol Coating Formation and Evaporation: Chamber Studies Using Black Carbon Seed Aerosol and the Single-Particle Soot Photometer, Aerosol Sci. Technol., 47, 326-347, https://doi.org/10.1080/02786826.2012.750712, 2013.

Mohr, C., Lopez-Hilfiker, F. D., Zotter, P., Prévôt, A. S. H., Xu, L., Ng, N. L., Herndon, S. C., Williams, L. R., Franklin, J. P., Zahniser, M. S., Worsnop, D. R., Knighton, W. B., Aiken, A. C., Gorkowski, K. J., Dubey, M. K., Allan, J. D., and Thornton, J. A.: Contribution of Nitrated Phenols to Wood Burning Brown Carbon Light Absorption in Detling, United Kingdom during Winter Time, Environmental Science & Technology, 47, 6316-6324, https://doi.org/10.1021/es400683v, 2013.

Onasch, T. B., Trimborn, A. M., Fortner, E. C., Jayne, J. T., Kok, G. L., Williams, L. R., Davidovits, P., and Worsnop, D. R.: Soot Particle Aerosol Mass Spectrometer: Development, Validation and Initial Application, Aerosol Science and Technology, 46, 804-817, https://doi.org/10.1080/02786826.2012.663948, 2012.

Peng, J., Hu, M., Guo, S., Du, Z., Zheng, J., Shang, D., Zamora, M. L., Zeng, L., Shao, M., Wu, Y.-S., Zheng, J., Wang, Y., Glen, C. R., Collins, D. R., Molina, M. J., and Zhang, R.: Markedly enhanced absorption and direct radiative forcing of black carbon under polluted urban environments, Proc. Natl. Acad. Sci. U. S. A., 113, 4266-4271, https://doi.org/10.1073/pnas.1602310113, 2016.

Phillips, S. M., and Smith, G. D.: Spectroscopic comparison of water- and methanol-soluble brown carbon particulate matter, Aerosol Science and Technology, 51, 1113-1121, https://doi.org/10.1080/02786826.2017.1334109, 2017.

Pokhrel, R. P., Wagner, N. L., Langridge, J. M., Lack, D. A., Jayarathne, T., Stone, E. A., Stockwell, C. E., Yokelson, R. J., and Murphy, S. M.: Parameterization of single-scattering albedo (SSA) and absorption Ångström exponent (AAE) with EC / OC for aerosol emissions from biomass burning, Atmos. Chem. Phys., 16, 9549-9561, https://doi.org/10.5194/acp-16-9549-2016, 2016.

Pokhrel, R. P., Beamesderfer, E. R., Wagner, N. L., Langridge, J. M., Lack, D. A., Jayarathne, T., Stone, E. A., Stockwell, C. E., Yokelson, R. J., and Murphy, S. M.: Relative importance of black carbon, brown carbon, and absorption enhancement from clear coatings in biomass burning emissions, Atmospheric Chemistry and Physics, 17, 5063-5078, https://doi.org/10.5194/acp-17-5063-2017, 2017.

790 Qin, Y. M., Tan, H. B., Li, Y. J., Li, Z. J., Schurman, M. I., Liu, L., Wu, C., and Chan, C. K.:
791 Chemical characteristics of brown carbon in atmospheric particles at a suburban site near
792 Guangzhou, China, Atmos. Chem. Phys., 18, 16409-16418, https://doi.org/10.5194/acp-18-16409-
793 2018, 2018.

794 Reid, J. S., Koppmann, R., Eck, T. F., and Eleuterio, D. P.: A review of biomass burning emissions
795 part II: intensive physical properties of biomass burning particles, Atmos. Chem. Phys., 5, 799-
796 825, https://doi.org/10.5194/acp-5-799-2005, 2005.

797 Sahu, L. K., Kondo, Y., Moteki, N., Takegawa, N., Zhao, Y., Cubison, M. J., Jimenez, J. L., Vay,
798 S., Diskin, G. S., Wisthaler, A., Mikoviny, T., Huey, L. G., Weinheimer, A. J., and Knapp, D. J.:
799 Emission characteristics of black carbon in anthropogenic and biomass burning plumes over
800 California during ARCTAS-CARB 2008, Journal of Geophysical Research-Atmospheres, 117,
801 https://doi.org/10.1029/2011jd017401, 2012.

802 Saleh, R., Hennigan, C. J., McMeeking, G. R., Chuang, W. K., Robinson, E. S., Coe, H., Donahue,
803 N. M., and Robinson, A. L.: Absorptivity of brown carbon in fresh and photo-chemically aged
804 biomass-burning emissions, Atmospheric Chemistry and Physics, 13, 7683-7693,
805 https://doi.org/10.5194/acp-13-7683-2013, 2013.

806 Saleh, R., Robinson, E. S., Tkacik, D. S., Ahern, A. T., Liu, S., Aiken, A. C., Sullivan, R. C.,
807 Presto, A. A., Dubey, M. K., Yokelson, R. J., Donahue, N. M., and Robinson, A. L.: Brownness
808 of organics in aerosols from biomass burning linked to their black carbon content, Nature Geosci,
809 7, 647-650, https://doi.org/10.1038/ngeo2220, 2014.

810 Saleh, R., Cheng, Z., and Atwi, K.: The Brown–Black Continuum of Light-Absorbing Combustion
811 Aerosols, Environmental Science & Technology Letters, ASAP,
812 https://doi.org/10.1021/acs.estlett.8b00305, 2018.

813 Schneider, J., Weimer, S., Drewnick, F., Borrmann, S., Helas, G., Gwaze, P., Schmid, O., Andreae,
814 M. O., and Kirchner, U.: Mass spectrometric analysis and aerodynamic properties of various types
815 of combustion-related aerosol particles, International Journal of Mass Spectrometry, 258, 37-49,
816 https://doi.org/10.1016/j.ijms.2006.07.008, 2006.

817 Schwarz, J. P., Gao, R. S., Spackman, J. R., Watts, L. A., Thomson, D. S., Fahey, D. W., Ryerson,
818 T. B., Peischl, J., Holloway, J. S., Trainer, M., Frost, G. J., Baynard, T., Lack, D. A., de Gouw, J.
819 A., Warneke, C., and Del Negro, L. A.: Measurement of the mixing state, mass, and optical size
820 of individual black carbon particles in urban and biomass burning emissions, Geophysical
821 Research Letters, 35, L13810, https://doi.org/10.1029/2008gl033968, 2008.

822 Sekimoto, K., Koss, A. R., Gilman, J. B., Selimovic, V., Coggon, M. M., Zarzana, K. J., Yuan, B.,
823 Lerner, B. M., Brown, S. S., Warneke, C., Yokelson, R. J., Roberts, J. M., and de Gouw, J.: High-
824 and low-temperature pyrolysis profiles describe volatile organic compound emissions from
825 western US wildfire fuels, Atmos. Chem. Phys., 18, 9263-9281, https://doi.org/10.5194/acp-18-
826 9263-2018, 2018.

827 Sengupta, D., Samburova, V., Bhattarai, C., Kirillova, E., Mazzoleni, L., Iaukea-Lum, M., Watts,
828 A., Moosmüller, H., and Khlystov, A.: Light absorption by polar and non-polar aerosol compounds
829 from laboratory biomass combustion, Atmos. Chem. Phys., 18, 10849-10867,
830 https://doi.org/10.5194/acp-18-10849-2018, 2018.

831 Shamjad, P. M., Tripathi, S. N., Thamban, N. M., and Vreeland, H.: Refractive Index and
832 Absorption Attribution of Highly Absorbing Brown Carbon Aerosols from an Urban Indian City-
833 Kanpur, Scientific Reports, 6, 37735, https://doi.org/10.1038/srep37735, 2016.

834 Shiraiwa, M., Kondo, Y., Iwamoto, T., and Kita, K.: Amplification of Light Absorption of Black
835 Carbon by Organic Coating, Aerosol Science and Technology, 44, 46-54,
836 https://doi.org/10.1080/02786820903357686, 2010.

837 Sumlin, B. J., Pandey, A., Walker, M. J., Pattison, R. S., Williams, B. J., and Chakrabarty, R. K.:
838 Atmospheric Photooxidation Diminishes Light Absorption by Primary Brown Carbon Aerosol
839 from Biomass Burning, Environmental Science & Technology Letters, 4, 540-545,
840 https://doi.org/10.1021/acs.estlett.7b00393, 2017.

841 Sumlin, B. J., Heinson, Y. W., Shetty, N., Pandey, A., Pattison, R. S., Baker, S., Hao, W. M., and
842 Chakrabarty, R. K.: UV–Vis–IR spectral complex refractive indices and optical properties of
843 brown carbon aerosol from biomass burning, Journal of Quantitative Spectroscopy and Radiative
844 Transfer, 206, 392-398, https://doi.org/10.1016/j.jqsrt.2017.12.009, 2018.

845 Wandinger, Ulla, Müller, Detlef, Böckmann, Christine, Althausen, Dietrich, Matthias, Volker,
846 Bösenberg, Jens, Weiß, Volker, Fiebig, Markus, Wendisch, Manfred, Stohl, Andreas, and
847 Ansmann, A.: Optical and microphysical characterization of biomass- burning and industrial-
848 pollution aerosols from- multiwavelength lidar and aircraft measurements, Journal of Geophysical
849 Research: Atmospheres, 107, LAC 7-1-LAC 7-20, https://doi.org/doi:10.1029/2000JD000202,
850 2002.

851 Washenfelder, R. A., Attwood, A. R., Brock, C. A., Guo, H., Xu, L., Weber, R. J., Ng, N. L., Allen,
852 H. M., Ayres, B. R., Baumann, K., Cohen, R. C., Draper, D. C., Duffey, K. C., Edgerton, E., Fry,
853 J. L., Hu, W. W., Jimenez, J. L., Palm, B. B., Romer, P., Stone, E. A., Wooldridge, P. J., and
854 Brown, S. S.: Biomass burning dominates brown carbon absorption in the rural southeastern
855 United States, Geophysical Research Letters, 42, 653-664,
856 https://doi.org/10.1002/2014GL062444, 2015.

857 Xie, M., Hays, M. D., and Holder, A. L.: Light-absorbing organic carbon from prescribed and
858 laboratory biomass burning and gasoline vehicle emissions, Scientific Reports, 7, 7318,
859 https://doi.org/10.1038/s41598-017-06981-8, 2017.

860 Yang, M., Howell, S. G., Zhuang, J., and Huebert, B. J.: Attribution of aerosol light absorption to
861 black carbon, brown carbon, and dust in China – interpretations of atmospheric measurements
862 during EAST-AIRE, Atmospheric Chemistry and Physics, 9, 2035-2050,
863 https://doi.org/10.5194/acp-9-2035-2009, 2009.

864 Zhang, X., Kim, H., Parworth, C., Young, D. E., Zhang, Q., Metcalf, A. R., and Cappa, C. D.:
865 Optical Properties of Wintertime Aerosols from Residential Wood Burning in Fresno, CA: Results
866 from DISCOVER-AQ 2013, Environmental Science & Technology, 50, 1681-1690,
867 https://doi.org/10.1021/acs.est.5b04134, 2016.

868

869

870

871 # 9 Tables

872 **Table 1.** Fuels by particle Class.

Class	Fuel	SSA range	[OA]/[BC] range
Class 1	Chaparral, canopy, litter (pine), building materials, excelsior	0.23-0.43	0.3-2.4
Class 2	Manzanita, Sage, litter (fir)	0.43-0.60	1.5-4.1
Type 3	Pine, fir, litter, canopy, juniper	0.60-0.74	6.6-20
Class 4	Pine, fir, canopy, rotten log, ceonothos	0.74-0.87	8.3-55
Class 5	Canopy (pine), rice, bear grass, duff	0.87-0.93	31-143
Class 6	Rotten log, duff, peat, dung	0.93-1.00	$431\text{-}10^5$

873

874

10 Figures

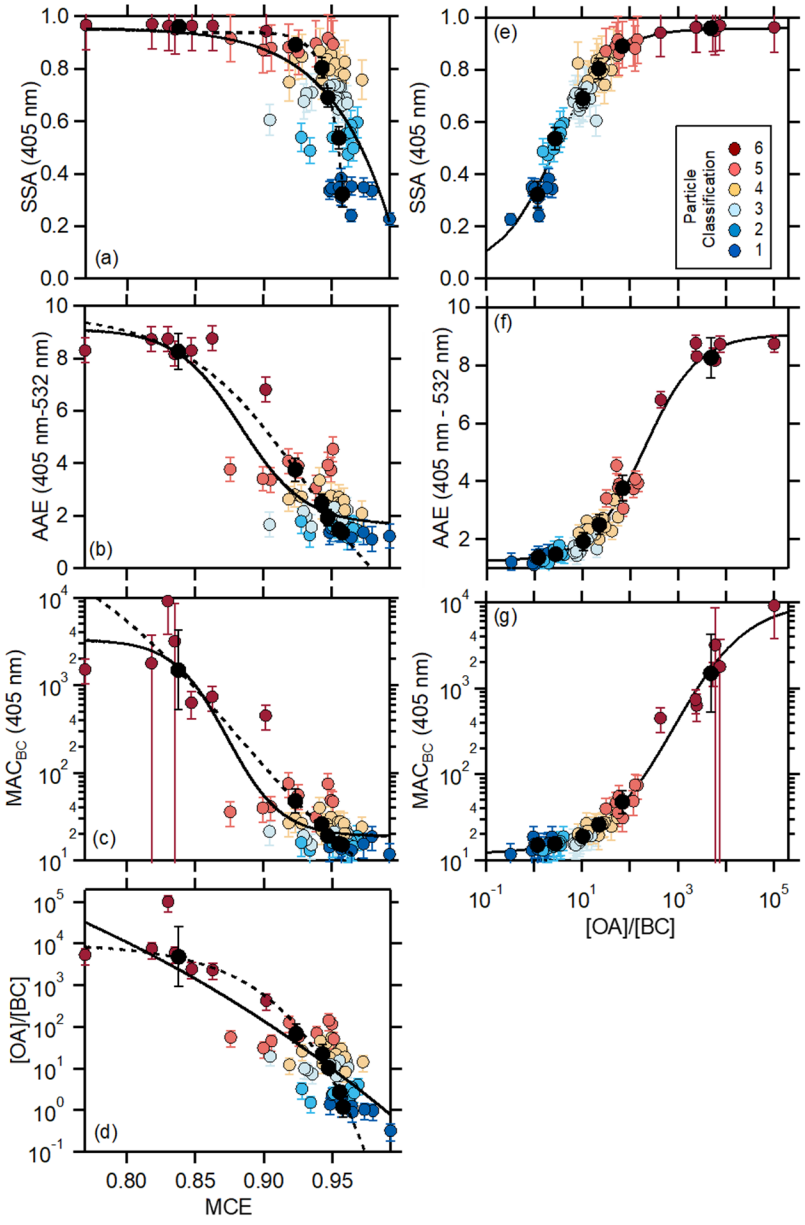

Figure 1. (left panels) Relationship between (a) the SSA_{405nm}, (b) the $AAE_{405\text{-}532}$, (c) the MAC_{BC}, and (d) the [OA]/[BC] mass ratio and the modified combustion efficiency, MCE. Results for individual burns are shown as points colored by the particle Class, and Class average values are shown as black circles. Uncertainties on the Class averages are 1σ based on measurement variability and uncertainties on for the individual burns are from error propagation of measurement uncertainties. The solid black lines are fits to the individual burns (colored points) while the dashed black lines are fits to the Class averages (Table S2). (right panels) Relationship between (e) the SSA_{405nm}, (f) the $AAE_{405\text{-}532}$, and (g) the MAC_{BC} on the [OA]/[BC] mass ratio. The solid black lines here are sigmoidal fits to the individual burns. Fits to the Class averages are similar.

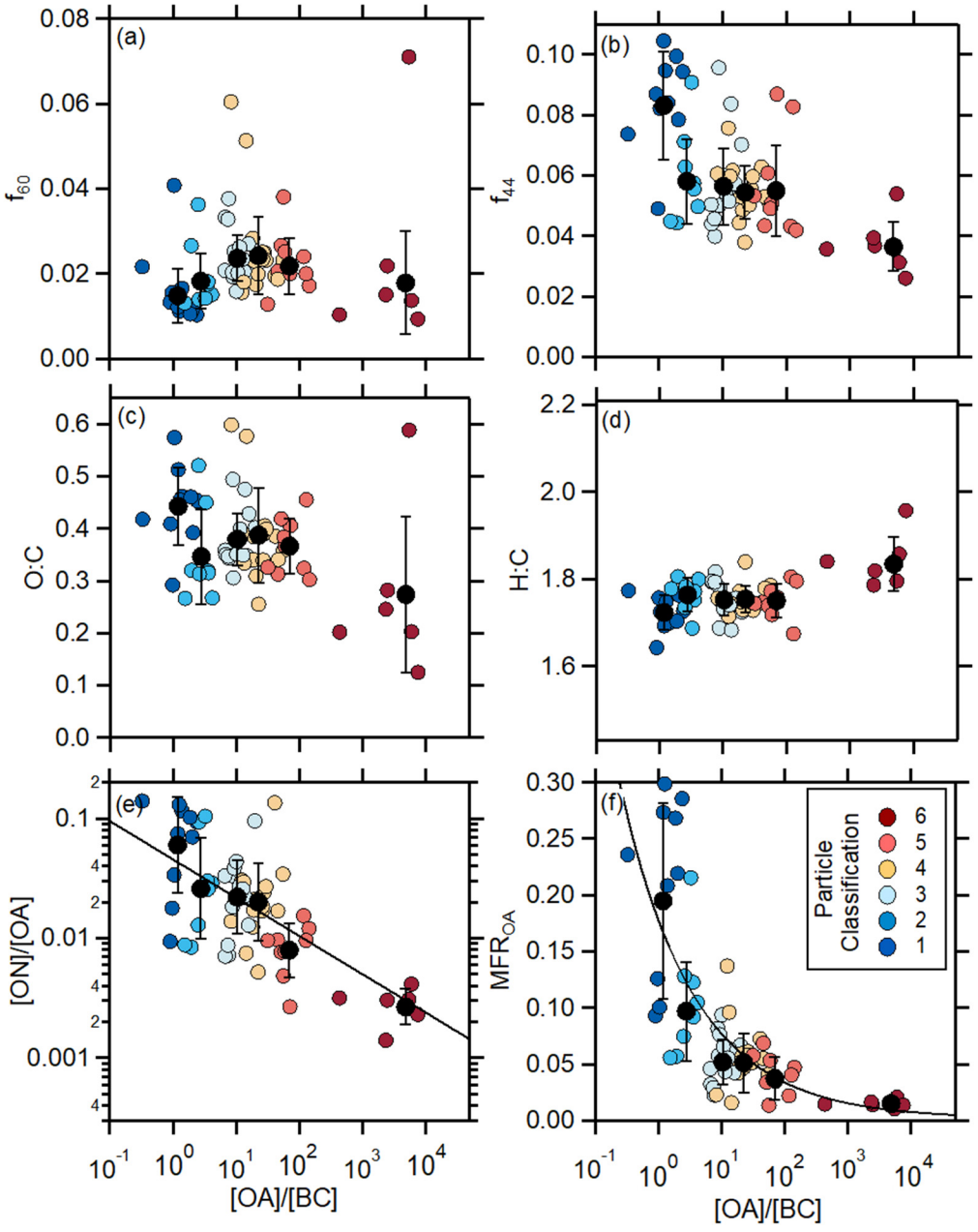

Figure 2. Dependence of (a) f_{60}, (b) f_{44}, (c) O:C, (d) H:C, (e) the nitrated organic fraction of OA, $f_{ON\text{-}OA}$, and (f) the OA volatility, characterized as the mass fraction remaining after heating. Results for individual burns are shown as points colored by the particle Class, and Class average values are shown as black circles. Uncertainties on the Class averages are 1σ based on measurement variability. For $f_{ON\text{-}OA}$ and MFR_{OA}, fits to the observations are shown (see text).

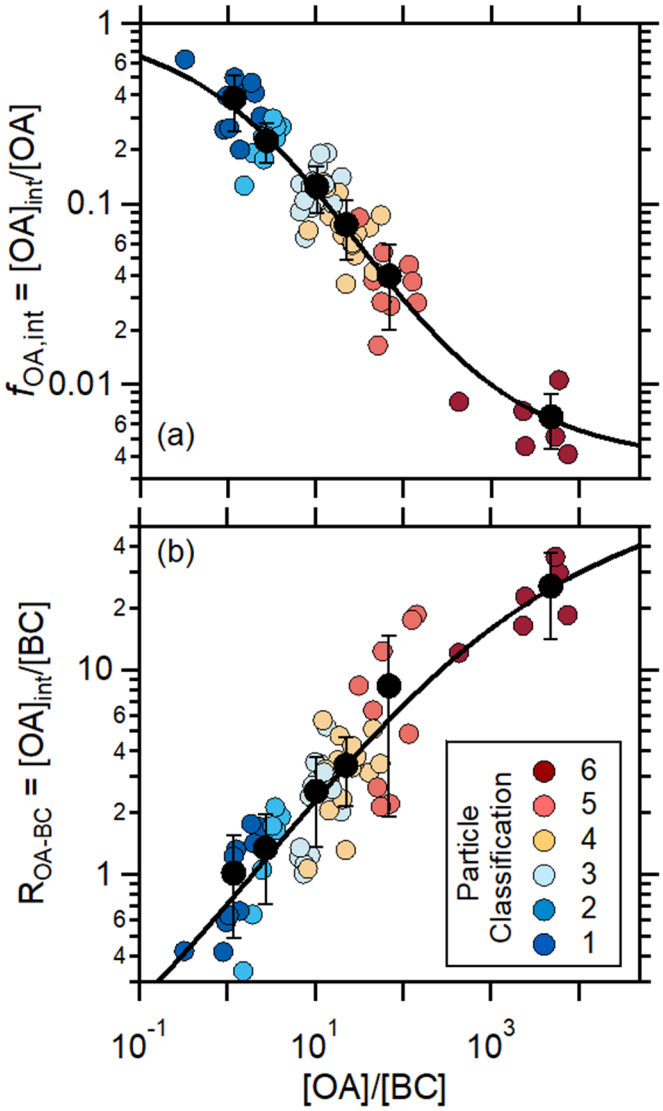

894

895 **Figure 3.** Relationship between (a) the fraction of OA that is internally mixed with BC, $f_{OA,int}$ and
896 (b) the OA-to-BC mass ratio for only the internally mixed OA, and the total [OA]/[BC] mass ratio.
897 Results for individual burns are shown as points colored by the particle Class, and Class average
898 values are shown as black circles. Uncertainties on the Class averages are 1σ based on
899 measurement variability. Black lines are sigmoidal fits to the data, in log-log space.

900

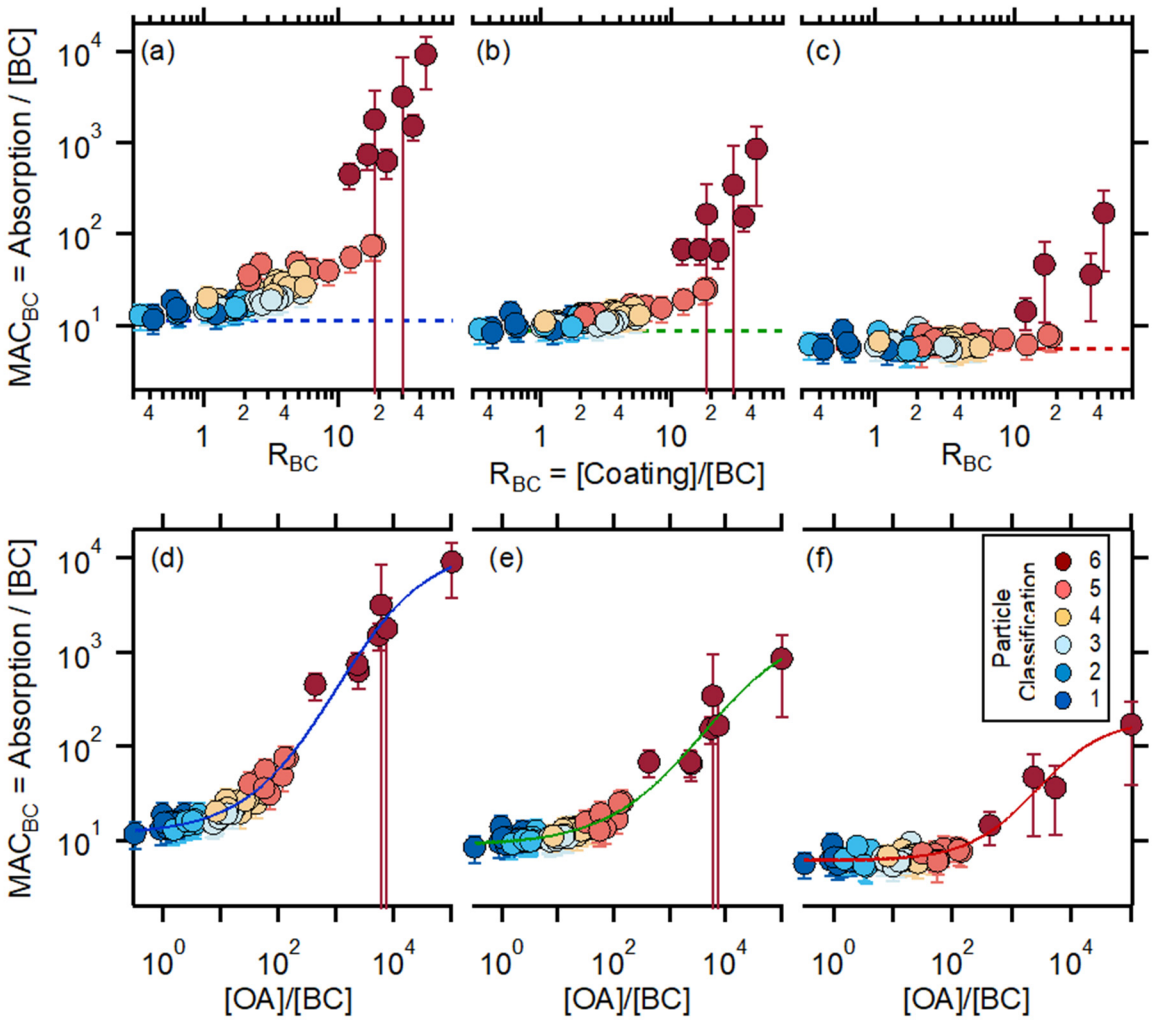

Figure 4. (Top Panels) The relationship between the wavelength-specific MAC_{BC} and the coating-to-BC mass ratio for (a) 405 nm, (b) 532 nm and (c) 781 nm. The horizontal dashed lines show the derived $MAC_{BC,pure}$ values. (Bottom Panels) The relationship between the wavelength-dependent MAC_{BC} and the total [OA]/[BC] mass ratio for (d) 405 nm, (e) 532 nm and (f) 781 nm. The lines are sigmoidal fits. Uncertainties for the individual burns are determined from error propagation. Graphs of the wavelength-specific MAC_{BC} versus [OA]/[BC] with each shown using independent y-axis scales are provided for comparison in **Figure S1**.

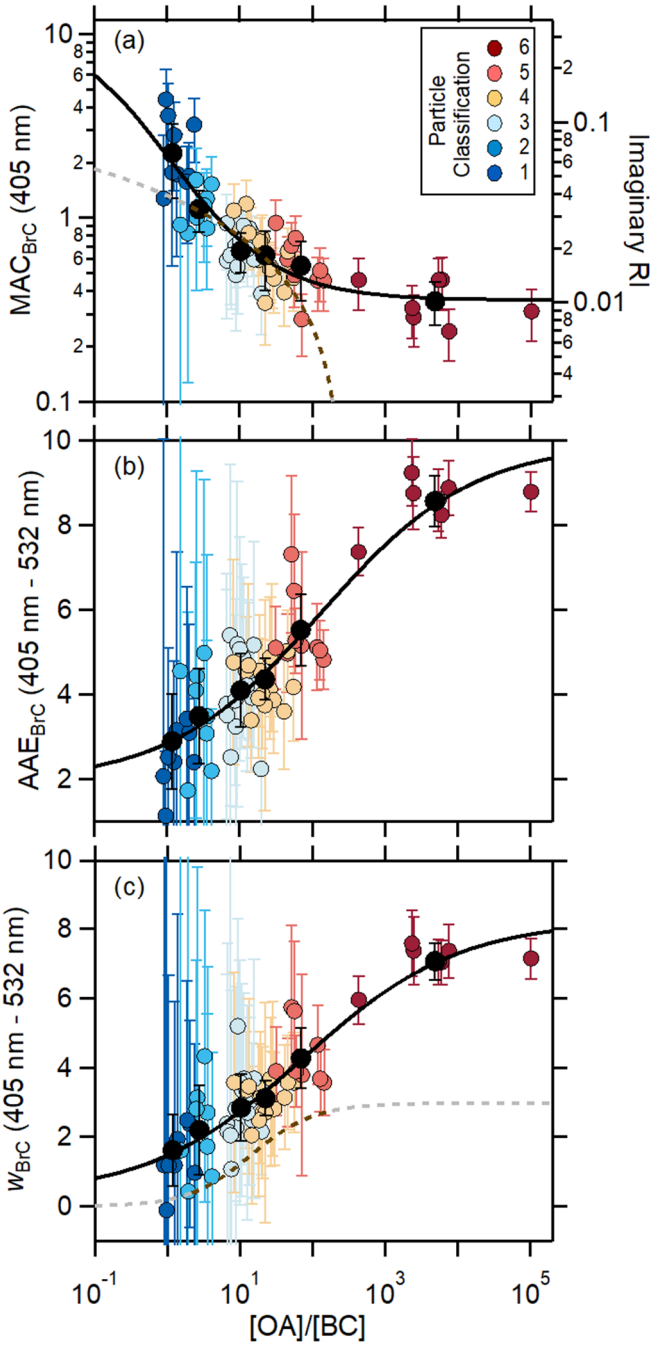

910

911 **Figure 5.** Relationship between (a) $MAC_{BrC,405nm}$, (b) $AAE_{BrC,405-532}$, and (c) $w_{BrC,405-532}$ and the
912 [OA]/[BC] mass ratio. The solid lines are sigmoidal fits to the observations, against
913 log([OA]/[BC]). The dashed lines are based on the parameterization of Saleh et al. (2014), with
914 the brown color indicating the measuring range in that study and the gray color extrapolated.
915 Results for individual burns are shown as points colored by the particle Class, and Class average
916 values are shown as black circles. Uncertainties on the Class averages are 1σ based on
917 measurement variability. Uncertainties for the individual burns are determined from error
918 propagation.

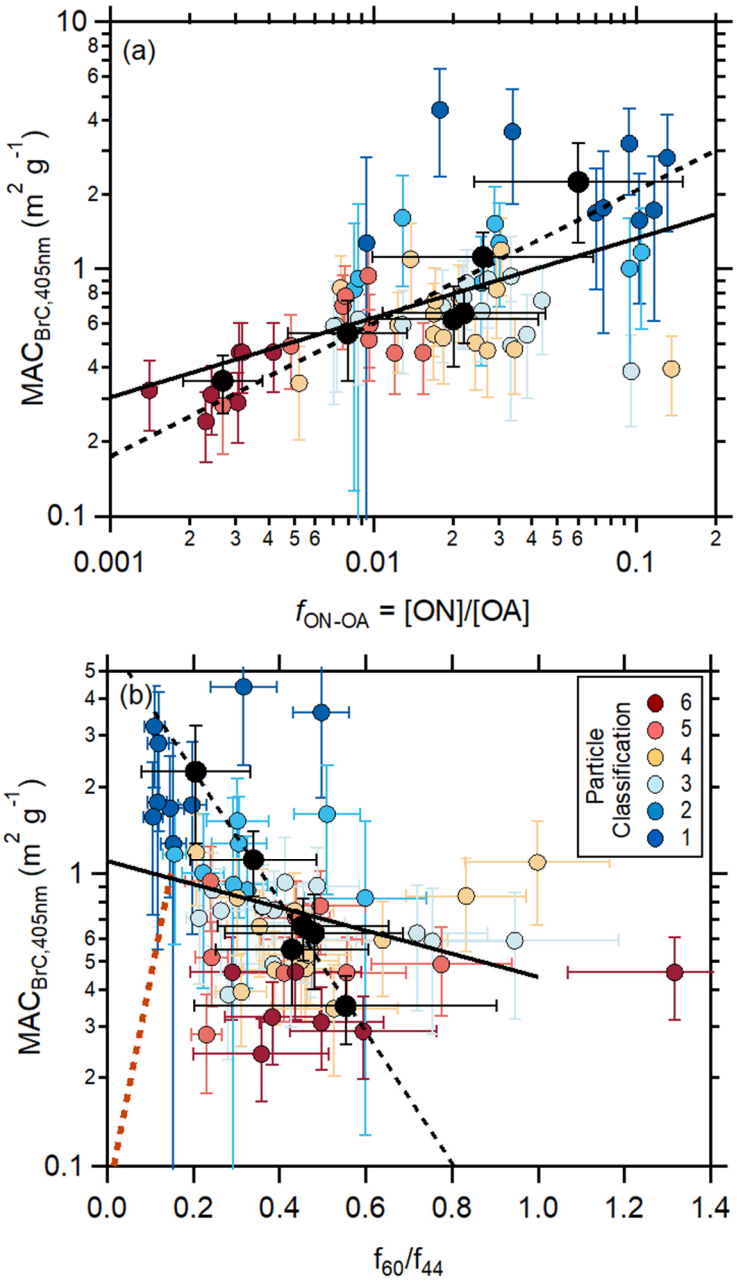

Figure 6. Relationship between the $MAC_{BrC,405nm}$ and (a) the nitrated organic fraction of total organic aerosol, f_{ON-OA}, and (b) the f_{60}/f_{44} ion ratio for organic aerosol. Results for individual burns are shown as points colored by the particle Class, and Class average values are shown as black circles. Uncertainties on the Class averages are 1σ based on measurement variability. Uncertainties for the individual burns are determined from error propagation. Solid black lines are fits to all burns and dashed black lines are fits to the Class averages. The dashed brown line in panel (b) is the relationship reported by Lack et al. (2013) for ambient particles in a biomass burning plume.

928

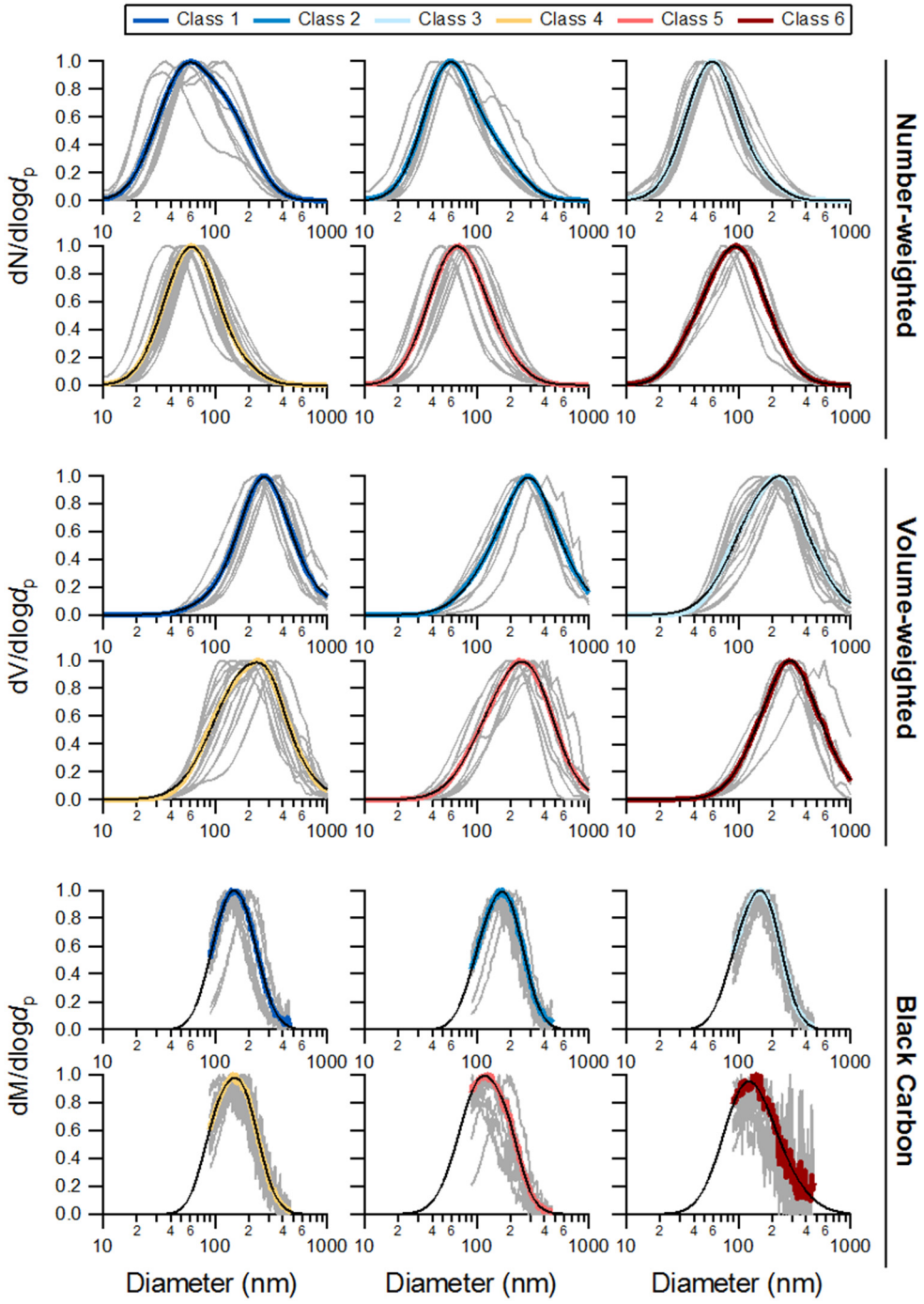

929

930 **Figure 7.** Class-specific total particle number-weighted (top) and volume-weighted (middle)
931 mobility size distributions, and the BC-only mass-weighted (bottom) size distribution. Individual
932 burns are shown in gray and class averages are shown as colors. Bimodal log-normal fits are thin
933 black lines. Note that the number-weighted and volume-weighted distributions are graphed versus
934 mobility diameter and the BC mass-weighted distribution against the BC volume equivalent
935 diameter.

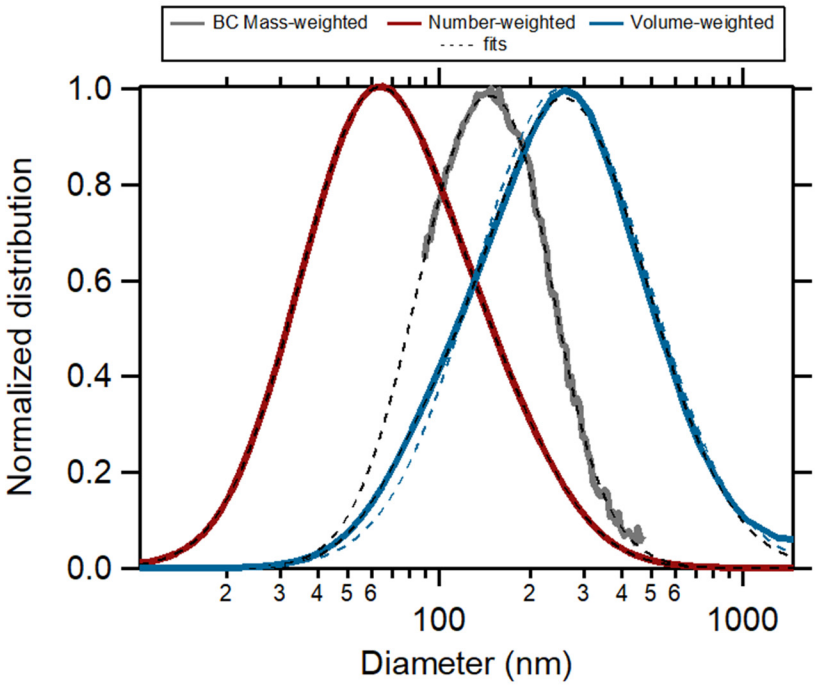

936

937 **Figure 8.** Average total particle number-weighted (red) and volume-weighted (blue) size
938 distributions and the BC-specific mass-weighted size distributions. Black dashed lines are bimodal
939 log-normal fits. The dashed blue line is the total particle volume-weighted distribution calculated
940 from a single-mode fit to the number-weighted distribution. Note that the number-weighted and
941 volume-weighted distributions are graphed versus mobility diameter and the BC mass-weighted
942 distribution against the BC volume equivalent diameter.

943

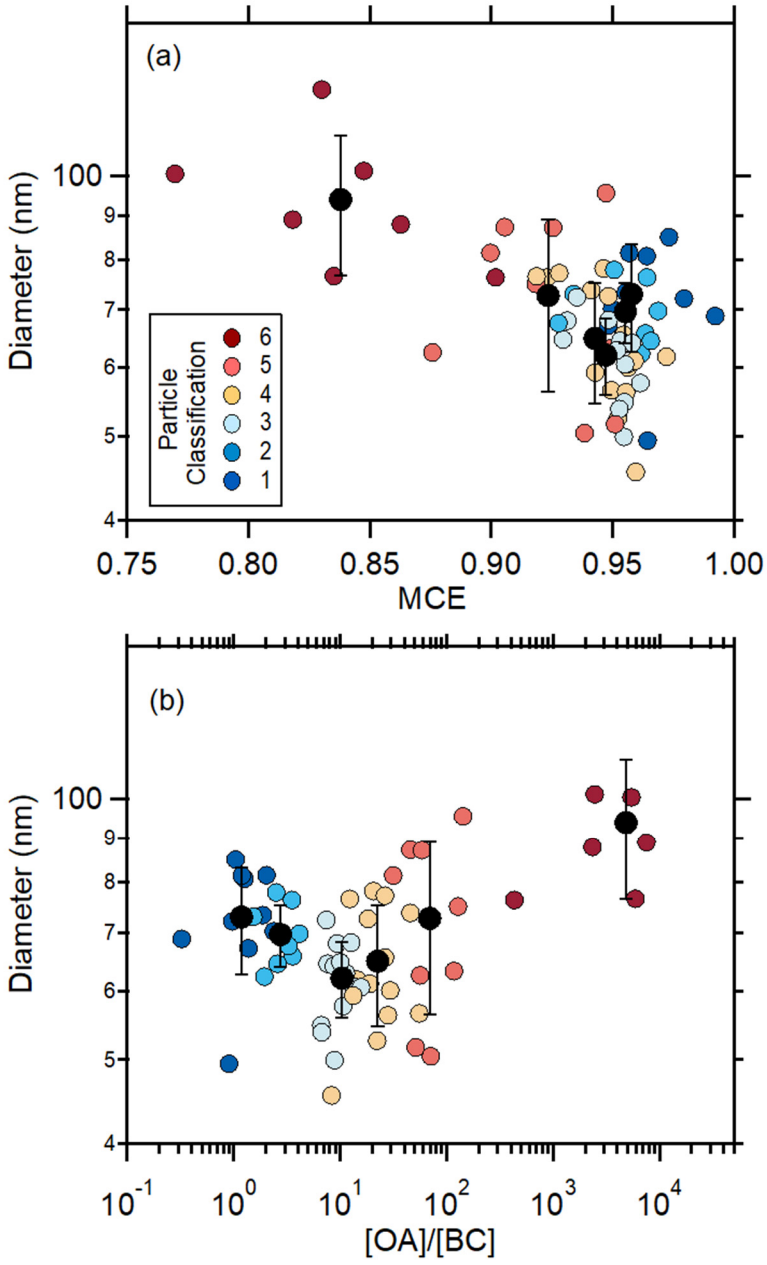

944

945 **Figure 9.** Relationship between number-weighted particle median diameter and (a) the MCE and
946 (b) the [OA]/[BC] ratio. Colored circles are for individual burns and black circles for particle class
947 averages.

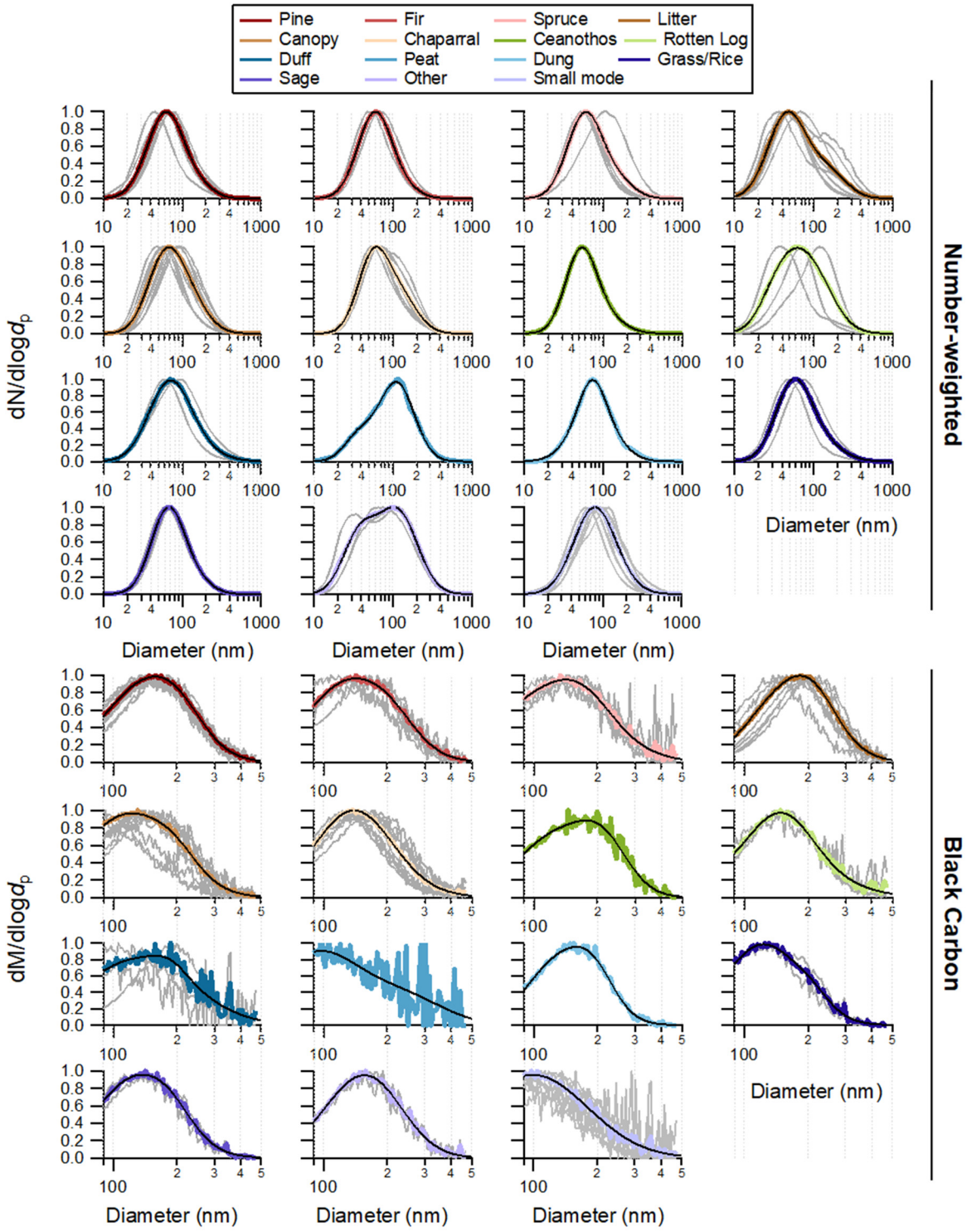

Figure 10. Normalized total particle number-weighted (top) and the BC-only mass-weighted (bottom) size distributions shown by fuel type (see legend). Individual burns are gray and averages for a fuel type colors. For some fuels there is only one size distribution. Bimodal log-normal fits are the black lines. The "other" category includes non-traditional biofuels, specifically building materials and excelsior.